

1 **Simulated retrievals for the remote sensing of CO<sub>2</sub>,**  
2 **CH<sub>4</sub>, CO, and H<sub>2</sub>O from geostationary orbit**

3  
4  
5

6 X. Xi<sup>1</sup>, V. Natraj<sup>2</sup>, R. L. Shia<sup>1</sup>, M. Luo<sup>2</sup>, Q. Zhang<sup>1</sup>, S. Newman<sup>1</sup>, S. P. Sander<sup>2</sup>, and Y. L.  
7 Yung<sup>1,2</sup>

8 <sup>1</sup>Environmental Science and Engineering, California Institute of Technology, Pasadena,  
9 California, USA

10 <sup>2</sup>Jet Propulsion Laboratory, California Institute of Technology, Pasadena, California, USA

11

12 Correspondence to: X. Xi (xixi@caltech.edu)

1 **Abstract**

2

3 The Geostationary Fourier Transform Spectrometer (GeoFTS) is designed to measure high-  
4 resolution spectra of reflected sunlight in three near-infrared bands centered around 0.76  $\mu\text{m}$ , 1.6  
5  $\mu\text{m}$ , and 2.3  $\mu\text{m}$  and to deliver simultaneous retrievals of column-averaged dry air mole fractions  
6 of  $\text{CO}_2$ ,  $\text{CH}_4$ ,  $\text{CO}$ , and  $\text{H}_2\text{O}$  (denoted  $X\text{CO}_2$ ,  $X\text{CH}_4$ ,  $X\text{CO}$ , and  $X\text{H}_2\text{O}$ , respectively) at different  
7 times of day over North America. In this study, we perform radiative transfer simulations over  
8 both clear-sky and all-sky scenes expected to be observed by GeoFTS and estimate the  
9 prospective performance of retrievals based on results from Bayesian error analysis and  
10 characterization.

11

12 We find that, for simulated clear-sky retrievals, the average retrieval biases and single-  
13 measurement precisions are  $< 0.2\%$  for  $X\text{CO}_2$ ,  $X\text{CH}_4$ , and  $X\text{H}_2\text{O}$ , and  $< 2\%$  for  $X\text{CO}$ , when the a  
14 priori values have a bias of 3% and an uncertainty of 3%. In addition, an increase in the amount  
15 of aerosols and ice clouds leads to a notable increase in the retrieval biases and slight worsening  
16 of the retrieval precisions. Furthermore, retrieval precision is a strong function of signal-to-noise  
17 ratio and spectral resolution. This simulation study can help guide decisions on the design of the  
18 GeoFTS observing system, which can result in cost-effective measurement strategies while  
19 achieving satisfactory levels of retrieval precisions and biases. The simultaneous retrievals at  
20 different times of day will be important for more accurate estimation of carbon sources and sinks  
21 on fine spatiotemporal scales and for studies to better understand the close coupling between the  
22 carbon and water cycles.

## 1 **1. Introduction**

2

3 The global carbon cycle has been significantly perturbed since the start of industrialization. The  
4 atmospheric concentrations of the greenhouse gases (GHG) carbon dioxide (CO<sub>2</sub>), methane  
5 (CH<sub>4</sub>), and the pollutant carbon monoxide (CO) have all increased substantially due to  
6 anthropogenic activities (IPCC, 2013). These potent greenhouse gases trap outgoing long-wave  
7 radiation and warm the Earth's atmosphere and surface. As surface temperature continues to rise,  
8 the global water cycle is also notably changed (IPCC, 2013). Being the most potent greenhouse  
9 gas, water vapor (H<sub>2</sub>O) is of crucial importance to climate studies. An accurate understanding of  
10 carbon storage in the atmosphere, oceans, and terrestrial biosphere, as well as the exchanges  
11 between these reservoirs and the coupling with the water cycle, is critical to confidently project  
12 the future evolution of climate and to support societal efforts to mitigate climate change.  
13 However, despite decades of research, the Earth's carbon budget, especially the changes in the  
14 carbon sinks, still remains uncertain on regional and global scales (Le Quéré et al., 2009; Le  
15 Quéré et al., 2014). In particular, two major challenges remain in balancing the carbon budget:  
16 quantifying uncertainty in fossil fuel CO<sub>2</sub> emissions (Le Quéré et al., 2009), and constraining the  
17 variability and uncertainty of land fluxes (Schimel et al., 2001; Houghton et al., 2007).

18

19 To tackle these challenges in carbon cycle studies, several satellite missions have been  
20 measuring the atmospheric concentrations of greenhouse gases such as CO<sub>2</sub> and CH<sub>4</sub>. For  
21 example, the Atmospheric Infrared Sounder (AIRS), whose main scientific goal is to improve  
22 weather forecasting, has been able to measure mid-tropospheric CO<sub>2</sub> and CH<sub>4</sub> since 2002  
23 (Aumann et al., 2003; Chahine et al., 2005; Chahine et al., 2008; Xiong et al., 2008). The  
24 SCanning Imaging Absorption spectroMeter for Atmospheric CartograpHY (SCIAMACHY)  
25 instrument was operational for measurements of atmospheric compositions from 2002 to 2012,  
26 with CO<sub>2</sub>, CH<sub>4</sub>, CO, and H<sub>2</sub>O as four of its target species (Buchwitz et al., 2004; Buchwitz et al.,  
27 2007; Schrijver et al., 2009; Schneising et al., 2011). The Greenhouse gases Observing SATellite  
28 (GOSAT), developed by the Japan Aerospace Exploration Agency and launched in January  
29 2009, is the world's first mission dedicated to the monitoring of CO<sub>2</sub> and CH<sub>4</sub> (Yokota et al.,  
30 2009; Butz et al., 2011; Yoshida et al., 2011). In addition, the Orbiting Carbon Observatory

1 (OCO)-2 mission, successfully launched in July 2014, now provides high-quality and worldwide  
2 column abundances of CO<sub>2</sub> (Crisp et al., 2004; Crisp et al., 2012).

3  
4 Flying in a Low Earth Orbit (LEO), these missions can achieve nearly global coverage in about  
5 sixteen days and offer monthly averaged retrievals of greenhouse gases. One exception is  
6 SCIAMACHY that had a revisit time of six days. The sources and sinks of greenhouse gases are  
7 then inferred through flux inversions (e.g., Baker et al., 2010; Nassar et al., 2011). However, the  
8 low spatiotemporal measurement densities of the current Earth observing system in LEO result  
9 in a lack of information about emissions on smaller spatiotemporal scales (Chevallier et al.,  
10 2005; Hungershoefer et al., 2010; Wecht et al., 2014). For example, localized emissions from  
11 forest fires and megacities vary over days or even hours. Furthermore, as the carbon and water  
12 cycles are closely coupled in the terrestrial biosphere, there is a significant scientific need to  
13 simultaneously study both on a daily basis.

14  
15 The Geostationary Fourier Transform Spectrometer (GeoFTS) combines an imaging Fourier  
16 Transform Spectrometer instrument with a geostationary Earth orbit vantage point and thereby  
17 promises to realize a transformational advance in carbon and water monitoring beyond the  
18 synoptic capability of the current LEO instruments. As a proposed mission at this point in time, it  
19 is designed to measure high-resolution spectra of reflected sunlight in near-infrared bands and to  
20 deliver simultaneous retrievals of column-averaged dry air mole fractions of CO<sub>2</sub>, CH<sub>4</sub>, CO, and  
21 H<sub>2</sub>O (denoted XCO<sub>2</sub>, XCH<sub>4</sub>, XCO, and XH<sub>2</sub>O, respectively) at different times of day over North  
22 America. A prototype of the instrument on top of Mount Wilson, in the San Gabriel Mountains  
23 just north of Los Angeles, California, has been collecting high-quality data over that megacity  
24 since August 2011 (Key et al., 2012; Fu et al., 2014; Wong et al., 2015). The main scientific  
25 objectives of GeoFTS are to:

- 26 1) Provide observations with the spatial and temporal density required to enable reliable flux  
27 inversions, which allow assessments of surface-atmosphere carbon exchange on scales that  
28 mirror fundamental carbon cycle processes. To better constrain the flux inversions, the  
29 requirements for single-sounding XCO<sub>2</sub>, XCH<sub>4</sub>, and XCO retrieval precisions are less than  
30 0.5% (~2 ppmv), 1% (~18 ppbv), and 10% (~12 ppbv), respectively (Rayner et al., 2001;  
31 Rayner et al., 2014).

- 1 2) Quantify the magnitude and spatiotemporal patterns of atmospheric signatures of  
2 anthropogenic CO<sub>2</sub>, CH<sub>4</sub>, and CO emissions (e.g., Newman et al., 2013).
- 3 3) Examine the close coupling between the carbon and water cycles with retrievals of XCO<sub>2</sub>,  
4 XCH<sub>4</sub>, XCO, and XH<sub>2</sub>O. Because water vapor is the dominant greenhouse gas and its  
5 amount in the atmosphere is controlled by temperature, it constitutes a positive feedback on  
6 climate (Bengtsson, 2010). The co-located retrievals of these trace gases could provide more  
7 information about how the amount of atmospheric water vapor might change when carbon  
8 fluxes change.

9  
10 Simulation studies have been done in the past to evaluate the design of proposed observing  
11 systems and have proven to be informative for the design of new missions. For example, Kuang  
12 et al. (2002) conducted an introductory study on the potential of using a 3-band spectrometric  
13 approach to accurately measure atmospheric CO<sub>2</sub> from space. The OCO-2 mission has adopted  
14 the measurement strategy pioneered by their simulation study. Buchwitz et al. (2013) developed  
15 an error parameterization scheme for the proposed CarbonSat mission and assessed atmospheric  
16 CO<sub>2</sub> and CH<sub>4</sub> retrieval errors in a simulated environment. Polonsky et al. (2014) conducted end-  
17 to-end simulated retrievals for the proposed geoCARB mission and found that accurate  
18 measurements of trace gases make it possible to monitor localized emission sources such as  
19 power plants.

20  
21 In this study, we perform radiative transfer simulations over both clear-sky and all-sky scenes  
22 expected to be observed by GeoFTS and estimate the prospective performance of retrievals  
23 based on results from Bayesian error analysis and characterization. This paper is structured as  
24 follows. Section 2 explains the methodology of simulated retrievals. Section 3 presents and  
25 discusses the results of column-averaged retrievals, their sensitivity to signal-to-noise ratio  
26 (SNR) and spectral resolution, and the influence of aerosols and clouds. Section 4 summarizes  
27 the major scientific contributions and some limitations of this study.

## 28 29 **2. Methodology**

1 This section presents the design of the observing system for GeoFTS, the set-up for the simulated  
2 retrievals, the forward model, the retrieval algorithm, and some diagnostics of the observing  
3 system.

## 4 5 **2.1 Design of the GeoFTS observing system**

6 The science objectives of GeoFTS require continuous coverage of bioactive land surfaces, as  
7 well as major population centers. It will cover the latitude range of 60°N to 60°S based on an  
8 assumed 95°W geostationary longitude. For the purposes of this study, we focus only on North  
9 America from 60°N to 30°N. Figure 1 shows a schematic diagram of the GeoFTS observing  
10 system. At a fixed position relative to Earth, an FTS with agile pointing optics can scan all of  
11 North America in any pattern. The spatial resolution is designed to match modeling scales: 10  
12 km for urban models and 10–50 km for regional flux inversion models. In addition, to maximize  
13 the fraction of clear-sky scenes, small footprints are needed. In GeoFTS, each 0.28×0.28 degree  
14 Instantaneous Field of View (IFoV) scene is imaged onto 64×64 pixels of a focal plane array,  
15 which provides a 2.7×2.7 km<sup>2</sup> size pixel footprint at nadir. The evolving atmospheric  
16 compositions are then inferred from the high-resolution spectra measured by the instrument. Fu  
17 et al. (2014) provide more details about a prototype of the instrument on Mount Wilson. The real  
18 instrument in space will be similar to the prototype, although the viewing geometry and the  
19 spectral resolution will be different from those for the ground-based instrument.

20  
21 For flux modeling, the temporal resolution needs to be paired to regional flux models, which use  
22 1 to 6 hour time steps and estimate daily fluxes (Wu et al., 2011). Considering that about 20–  
23 30% of the scenes over North America are without excessive aerosol and cloud loadings (Bréon  
24 et al., 2005), and taking into account the time steps used in flux models, at least four revisits per  
25 day are required. This revisit frequency requires GeoFTS to scan all of North America in about  
26 three hours when there is sufficient reflected sunlight to be measured. This will result in at most  
27 four useful measurements each day, thus capturing the diurnal variations of trace gases. An  
28 integration time of about one minute for each footprint should give a SNR of about 300. The  
29 scanning pattern shown in Fig. 1 is one of the many possible options available for GeoFTS.  
30 Faster revisit intervals are possible but involve trade-offs between SNR, spatial resolution, and  
31 geographic coverage.

1  
2 Three spectral bands are chosen to meet the GeoFTS science objectives. Table 1 shows the  
3 spectral bands used and the target species in each band. Band 1A is used for retrievals of CH<sub>4</sub>,  
4 CO, and H<sub>2</sub>O and Band 1B for CH<sub>4</sub>, CO<sub>2</sub>, and H<sub>2</sub>O. Band 2 is the O<sub>2</sub> A-band, which provides  
5 information about surface pressure, aerosols, and clouds (Crisp et al., 2004).

6

## 7 **2.2 Set-up for simulated retrievals**

8 After designing the observing system, studies need to be performed to evaluate whether this  
9 specific design will meet the requirements for single-sounding XCO<sub>2</sub>, XCH<sub>4</sub>, and XCO retrieval  
10 precisions. This is done through simulated retrievals, as illustrated in Fig. 2. We use realistic  
11 atmospheric profiles from the GEOS-CHEM global 3-D chemical transport model (Bey et al.,  
12 2001), with line positions and strengths obtained from the HITRAN 2008 molecular  
13 spectroscopic database. These are then input to a Line-By-Line Radiative Transfer Model  
14 (LBLRTM) (Clough et al., 2005) to generate the optical depths (ODs). The state-of-the-art  
15 Vector LInearized Discrete Ordinate Radiative Transfer (VLIDORT) model (Spurr, 2006)  
16 generates the synthetic radiance data after its model output is convolved with the instrument line  
17 shape (ILS) and white Gaussian measurement noise is added. A combination of a two-stream  
18 (2S) multiple scattering and an exact single scattering (ESS) model, henceforth referred to as the  
19 2S-ESS model, generates the modeled radiances for the retrieval. The 2S-ESS model also  
20 accounts for scattering effects of aerosols and clouds (Spurr and Natraj, 2011; Natraj, 2013),  
21 albeit not as accurately as VLIDORT. The differences between the VLIDORT and 2S-ESS  
22 models give a conservative representation of the forward model error in real retrievals.

23

24 The atmospheric profile used to generate the synthetic data is regarded as the “truth”. In  
25 retrievals where we do not know the “truth”, we first have some prior knowledge about the  
26 concentration of gases in the air column,  $\mathbf{x}_a$ . This a priori is used as input to the LBLRTM and  
27 2S-ESS models to generate the modeled radiances. The state vector  $\mathbf{x}$  is updated iteratively until  
28 the modeled radiances match the synthetic data adequately. If and when the two spectra do  
29 match, the state vector  $\mathbf{x}$  is then called the “retrieved” state.

30

1 Ten test locations in North America are chosen over a significant range of latitudes and  
2 longitudes on 26 and 30 July 2006. These two days are a Wednesday and a Sunday, respectively,  
3 thus accounting for the weekday-weekend variations in anthropogenic emissions. We will show  
4 specific results from Location 1 in Central California and retrieval statistics based on all ten  
5 locations. The original 116-level atmospheric profiles from the GEOS-CHEM model are  
6 interpolated to 20 carefully chosen levels. The Solar Irradiance Reference Spectra (SIRS)  
7 (Woods et al., 2009) is linearly interpolated to the wavenumbers in the GeoFTS spectral bands.  
8 For simplicity, surface reflection is assumed to be Lambertian. Broadband surface emissivity for  
9 each location is obtained from spaceborne measurements (Jacob et al., 2004).

### 11 **2.2.1 Forward model**

12 A forward model is a function that translates the concentration of gases in the atmosphere to the  
13 upwelling radiances measured by an instrument in space. In this study, there are two components  
14 to the forward model. The first component is the LBLRTM model that takes in an atmospheric  
15 profile and computes the ODs of each gaseous species based on spectroscopic information in the  
16 HITRAN 2008 database (Rothman et al., 2009). The absorption cross section ( $\sigma$ ) from the  
17 LBLRTM, the concentration of the gaseous species ( $[C]$ ) at various atmospheric heights ( $z$ ), and  
18 the total column-integrated OD of the gas ( $\tau$ ) are related as follows:

$$19 \quad \tau = \int_0^{\infty} \sigma \cdot [C] dz \quad (1)$$

20 Figure 3 shows the ODs of the four target species. CO<sub>2</sub>, CH<sub>4</sub>, and H<sub>2</sub>O absorb strongly in these  
21 spectral bands. Although CO only absorbs weakly, its absorption strength is sufficient for good  
22 retrievals in clear-sky conditions, as will be shown in Sec. 3.1. For all-sky retrievals, four types  
23 of aerosols (black carbon, organic carbon, seasalt, and sulphate) with realistic vertical profiles  
24 and diurnal variations are taken from GEOS-CHEM model output and introduced into the model  
25 atmosphere. Based on cloud observations from the CALIPSO mission (Winker et al., 2010), we  
26 also introduce a small amount of ice clouds to regions near the tropopause. The optical properties  
27 of both aerosols and ice clouds are calculated using Mie theory with parameterized Gamma  
28 particle size distributions (Heymsfield et al., 2002).

29  
30 The second component of the forward model is the radiative transfer model (VLIDORT for  
31 generating synthetic data and 2S-ESS for retrieval). Both models take in the same optical depths



1 of all the absorbing and scattering species (GHG, aerosols, and ice clouds) and compute the  
2 upwelling radiances based on the viewing geometry, the solar irradiance, and other auxiliary  
3 parameters. The zenith and azimuth angles of the Sun and the satellite are computed for each  
4 location at different times of day. The main difference between the two models is the better  
5 characterization of the scattering effects of aerosols and clouds in VLIDORT. This  
6 comprehensive radiative transfer model can use any number of computational quadrature angles  
7 (“streams”) for the discrete ordinates calculation and we employ 16 streams in our calculations.  
8 Both models are run with a spectral resolution of  $0.05 \text{ cm}^{-1}$ . Then, these high-resolution spectra  
9 are convolved with the GeoFITS ILS function to produce low-resolution spectra ( $0.25 \text{ cm}^{-1}$ ) (see  
10 Fig. 2 of Fu et al., 2014 for the ILS). The radiances generated from VLIDORT, with  
11 measurement noise added in, mimic the measurements that GeoFITS would make from the  
12 geostationary orbit. The outputs from 2S-ESS are the modeled radiances used in retrievals and  
13 they do not contain any measurement noise. Initially, the SNR is set at 300 and the spectral  
14 resolution at  $0.25 \text{ cm}^{-1}$ . These two parameters can be changed in the actual design of the  
15 observing system. The choices of SNR and spectral resolution and their impact on the retrieval  
16 results are discussed in Sec. 3.3.

17  
18 Several assumptions have been made in the forward model. It has been assumed that the  
19 spectroscopic parameters and the ILS are known with certainty and the surface is Lambertian. In  
20 reality, uncertainties in these variables would lead to retrieval errors (e.g., Wunch et al., 2011; Fu  
21 et al., 2014). In addition, no micro-windows are used in this study. They could be selected in the  
22 future to alleviate the problem of interference among the retrieved parameters and to speed up  
23 the numerical computations (e.g., Rodgers, 1998; Vidot et al., 2009; Kuai et al., 2010).

24

### 25 **2.2.2 Retrieval algorithm**

26 We use a non-linear Maximum A Posteriori (MAP) method to iteratively retrieve the state vector  
27  $\mathbf{x}$  (Rodgers, 2000). This method for retrieval has been widely used for GOSAT (Yoshida et al.,  
28 2011), Tropospheric Emission Spectrometer, and OCO-2 (Kuang et al., 2002; Connor et al.,  
29 2008; O’Dell et al., 2012; Crisp et al., 2012). The state vector  $\mathbf{x}$ , model parameters  $\mathbf{b}$ , and error  $\mathbf{e}$   
30 are related to the measurement vector  $\mathbf{y}$  by a forward model  $\mathbf{F}$ :

$$31 \quad \mathbf{y} = \mathbf{F}(\mathbf{x}, \mathbf{b}) + \mathbf{e} \quad (2)$$

1 The model parameters include trace gas spectroscopy and geometric and optical properties of  
 2 aerosols and clouds. The errors include both the forward model error and the instrument noise.  
 3 The goal of the non-linear MAP method is to minimize the Bayesian least-squares cost function,  
 4 which is defined as follows:

$$5 \quad J(\mathbf{x}) = [\mathbf{y} - \mathbf{F}(\mathbf{x}, \mathbf{b})]^T \mathbf{S}_e^{-1} [\mathbf{y} - \mathbf{F}(\mathbf{x}, \mathbf{b})] + (\mathbf{x} - \mathbf{x}_a)^T \mathbf{S}_a^{-1} (\mathbf{x} - \mathbf{x}_a) \quad (3)$$

6  $\mathbf{S}_a$  and  $\mathbf{S}_e$  are the error covariance matrices for the a priori and the measurement, respectively.  $\mathbf{S}_e$   
 7 is assumed to be a diagonal matrix with values of the square of the noise.  $\mathbf{x}$  and  $\mathbf{x}_a$  are the true  
 8 state and the a priori, respectively. The Levenberg-Marquardt method (Levenberg, 1944;  
 9 Marquardt, 1963) is used to obtain stable retrieval results within a trust region for nonlinear  
 10 least-squares problems. In each iteration, the  $(i+1)^{\text{th}}$  state vector,  $\mathbf{x}_{i+1}$ , is related to the  $i^{\text{th}}$  state  
 11 vector,  $\mathbf{x}_i$ , as follows:

$$12 \quad \mathbf{x}_{i+1} = \mathbf{x}_i + [(1 + \gamma)\mathbf{S}_a^{-1} + \mathbf{K}_i^T \mathbf{S}_e^{-1} \mathbf{K}_i]^{-1} \{ \mathbf{K}_i^T \mathbf{S}_e^{-1} [\mathbf{y} - \mathbf{F}(\mathbf{x}_i)] - \mathbf{S}_a^{-1} [\mathbf{x}_i - \mathbf{x}_a] \} \quad (4)$$

13 The parameter  $\gamma$  is set at 10 initially and updated after each iteration.  $\mathbf{F}(\mathbf{x}_i)$  is the forward model  
 14 output based on the state vector  $\mathbf{x}_i$ .  $\mathbf{K}_i$  ( $\delta\mathbf{F}(\mathbf{x}_i)/\delta\mathbf{x}_i$ ) is a Jacobian matrix that describes how the  
 15 modeled radiances change given an infinitesimal change in  $\mathbf{x}_i$ . It is computed using the finite  
 16 difference method. The iterations stop when each element of  $\mathbf{x}_{i+1}$  differs from the corresponding  
 17 one in  $\mathbf{x}_i$  by less than 0.001. Typically, it takes five to ten iterations for retrievals to converge to  
 18 stable results. Since this study is meant to serve as a proof of concept, the state vector is slightly  
 19 simpler than that anticipated to be used in the real retrievals. The state vector is defined in the  
 20 following way:

$$21 \quad \mathbf{x} = \begin{bmatrix} \eta(\text{CO}_2) \\ \eta(\text{CH}_4) \\ \eta(\text{CO}) \\ \eta(\text{H}_2\text{O}) \\ \eta(\text{T}) \\ \eta(\text{p}) \\ \eta(\epsilon) \\ \eta(\text{fs}) \\ \eta(\text{zo}) \end{bmatrix} \text{ for total column retrieval in clear sky conditions} \quad (5)$$

22 Here  $\eta$  stands for the multiplicative scaling factor retrieved for the atmospheric profile and other  
 23 parameters (T: temperature profile; p: pressure profile;  $\epsilon$ : broadband surface emissivity; fs:  
 24 frequency shift; zo: zero-level offset). As surface albedo is equal to one minus surface emissivity  
 25 and varies from site to site, by retrieving a scaling factor for surface emissivity, we retrieve

1 surface albedo indirectly. For each element in the state vector, the a priori is biased 3% with  
 2 respect to the true state, so as to allow easy comparison among retrieved values. The a priori one-  
 3 sigma ( $1\sigma$ ) error is also set at 3%, thus providing a fairly loose constraint on the a priori and  
 4 making the retrieval dependent on the measurement rather than the prior knowledge. Note that  
 5 the a priori constraints are small compared to the true uncertainties of  $\text{XH}_2\text{O}$  and  $\text{XCO}$ . More  
 6 realistic a priori values will be used in operational retrievals. For this simulation study, we  
 7 choose to set all of the a priori biases and errors to 3% so as to compare the retrieval results for  
 8 all four target species. All the elements are assumed to be independent of each other, i.e.,  $\mathbf{S}_a$  is  
 9 diagonal. The retrieved state vector can be expressed as:

$$10 \quad \hat{\mathbf{x}} = \mathbf{A}\mathbf{x} + (\mathbf{I}_n - \mathbf{A})\mathbf{x}_a + \mathbf{G}\mathbf{e} \quad (6)$$

11 The first term on the right hand side,  $\mathbf{A}\mathbf{x}$ , represents the contribution of the true state to the  
 12 retrieved state. The averaging kernel  $\mathbf{A}$  is defined as:

$$13 \quad \mathbf{A} = \frac{\partial \hat{\mathbf{x}}}{\partial \mathbf{x}} = (\mathbf{K}^T \mathbf{S}_e^{-1} \mathbf{K} + \mathbf{S}_a^{-1})^{-1} \mathbf{K}^T \mathbf{S}_e^{-1} \mathbf{K} = \mathbf{G}\mathbf{K} \quad (7)$$

14 It quantifies the relative contribution to the retrieval from the true state, compared to that from  
 15 the a priori. Correspondingly,  $(\mathbf{I}_n - \mathbf{A})$  represents the relative contribution to the retrieval from the  
 16 a priori. The second term,  $(\mathbf{I}_n - \mathbf{A})\mathbf{x}_a$ , is also known as the smoothing error because it smoothes  
 17 the solution towards the a priori. In the third term,  $\mathbf{G}$  stands for the gain matrix and  $\mathbf{G}\mathbf{e}$  represents  
 18 the retrieval error due to the random instrument noise and the forward model error. The error  
 19 covariance matrix for the retrieved state,  $\hat{\mathbf{S}}$ , quantifies the uncertainties in the retrieval based on  
 20  $\mathbf{S}_a$ ,  $\mathbf{S}_e$ , and  $\mathbf{K}$ :

$$21 \quad \hat{\mathbf{S}} = (\mathbf{K}^T \mathbf{S}_e^{-1} \mathbf{K} + \mathbf{S}_a^{-1})^{-1} \quad (8)$$

22 The square roots of its diagonal values give the  $1\sigma$  uncertainty of the retrievals.

23

### 24 **2.3 Diagnostics of the observing system**

25 In order to examine whether the design of the GeoFTS observing system would result in precise  
 26 trace gas retrievals, we implement the following diagnostics (Rodgers, 2000):

27

- 28 • Jacobian ( $\mathbf{K}$ ): it is the sensitivity of the modeled radiances to the state vector. A large Jacobian  
 29 indicates that a gaseous species absorbs strongly in the spectral band.

- 1 • Averaging Kernel (**A**): it quantifies the relative contribution to the retrieval from the true state,  
2 compared to that from the a priori. Ideally, it should be close to unity.
- 3 • Degrees of Freedom for signal (DoF): it describes the number of useful independent quantities  
4 there are in a measurement.  $\text{DoF} = \text{trace}(\mathbf{A})$ .
- 5 • Information Content ( $H$ ): it quantitatively describes how well the measurements increase our  
6 confidence in the estimation of the atmospheric state relative to the prior knowledge. As a  
7 scalar quantity,  $H$  is useful for characterizing and comparing observing systems.  
8 Mathematically, it is defined as:

$$9 \quad H = \frac{1}{2} \ln(|\hat{\mathbf{S}}^{-1} \mathbf{S}_a|) \quad (9)$$

- 10 • Retrieval bias: it is defined as the absolute percentage difference between the retrieval and the  
11 truth.
- 12 • Single-measurement precision: it is the  $1\sigma$  uncertainty of the retrieval  $\sigma_p$ , where p stands for the  
13 posterior state.
- 14 • Uncertainty Reduction (UR): it is defined as  $(\sigma_a - \sigma_p)/\sigma_a \times 100\%$ , where  $\sigma_a$  and  $\sigma_p$  stand for  
15 uncertainty of the a priori and the a posteriori, respectively.

16

### 17 **3. Results and discussion**

18

#### 19 **3.1 Simulated retrievals in clear sky conditions**

20 For clear-sky retrievals, the forward model generates the upwelling radiances based on the trace  
21 gas atmospheric profiles and other auxiliary parameters. Figure 4 illustrates the modeled  
22 radiances at four times of day at Location 1, a test location in Central California. As expected,  
23 the reflected sunlight captured by GeoFTS will be more intense at 12pm and 3pm and less so at  
24 9am and 6pm. This indicates that radiative transfer models dedicated to geostationary  
25 measurements can realistically simulate the diurnal variations of radiances.

26

27 Figure 5 shows the Jacobians for the four target species.  $\text{CO}_2$ ,  $\text{CH}_4$ , and  $\text{H}_2\text{O}$  absorb strongly in  
28 the two bands, while the  $\text{CO}$  absorptions are much weaker. The relative absorption strengths  
29 suggest that the retrieval results are likely to be better for  $\text{CO}_2$ ,  $\text{CH}_4$ , and  $\text{H}_2\text{O}$ . Through the  
30 iterative retrieval algorithm, a fit is obtained between the modeled radiances and the synthetic  
31 data. Figure 6 shows a sample spectral fit and residuals in all spectral bands. The fact that the

1 residuals fluctuate randomly around zero and follow an approximate Gaussian distribution (not  
2 shown) indicates that most of the information from the spectra has been extracted. Minor  
3 inaccuracies in the retrieved state result in some small spikes in the residuals. If the forward  
4 model is perfect and the SNR is 300, the theoretical lower limit for the root-mean-square (rms)  
5 value of the residuals is approximately 0.33%. The real rms values of the residuals from this  
6 simulated retrieval are close to the theoretical value, implying that most of the residuals are due  
7 to the random instrument noise, and not the forward model error.

8  
9 The averaging kernel approaches a unitary matrix (not shown). This indicates that most of the  
10 elements in the retrieved state are sensitive to the true state. Since the state vector for clear-sky  
11 retrievals contains 9 elements, as shown in Eq. (5), the theoretical upper limit for DoF is 9.  
12 Through simulated retrievals, the real DoF is calculated to be around 8.7. It falls slightly short of  
13 9 because of the relatively weak absorption of CO. The information content is around 42. This  
14 validates our expectation that the spectral measurements significantly improve our knowledge of  
15 the atmospheric state.

16  
17 Figure 7 summarizes the statistics of the retrieval results at ten locations over the two test days.  
18 There are a total of  $10 \text{ (locations)} \times 2 \text{ (days)} \times 4 \text{ (times of day)} = 80$  test cases and there is one  
19 simulated retrieval for each test case. The error bars show the standard deviations of the results  
20 over the ten locations. Most of the retrievals are highly accurate and precise in clear-sky  
21 conditions. The average retrieval biases and single-measurement precisions are  $< 0.2\%$  for  
22  $\text{XCO}_2$ ,  $\text{XCH}_4$ , and  $\text{XH}_2\text{O}$ , and  $< 2\%$  for XCO. The retrieval results for  $\text{XCO}_2$  and  $\text{XCH}_4$  are  
23 comparable to simulated retrievals by Polonsky et al. (2012), which examined  $\text{XCO}_2$ ,  $\text{XCH}_4$ , and  
24 XCO retrievals using similar spectral bands and the OCO simulator. The biases in XCO  
25 retrievals in their study are larger than the results presented here. This is mainly due to different  
26 smoothing errors based on different a priori values. As expected, our simulation results show  
27 smaller biases and better precisions than those in real retrievals (e.g., Fu et al., 2014; Crisp et al.,  
28 2012), partly because of the assumptions discussed in Sec. 2.2.1 and the different spectral bands  
29 used.

30

1 For gases that absorb weakly, the absolute value of the single-measurement precision might not  
2 be indicative of the retrieval performance. The results here are based on a priori biased 3% from  
3 the truth and having a 3% uncertainty. As CO absorbs weakly in the chosen spectral bands, the  
4 XCO retrievals are relatively more dependent on the a priori. If the a priori were further away  
5 from the truth and having a higher uncertainty, the single-measurement precision would get  
6 worse accordingly. This makes uncertainty reduction (UR) a more useful quantity as a diagnostic  
7 of the observing system.

8

9 The retrievals reduce the average uncertainty in XCO<sub>2</sub>, XCH<sub>4</sub>, XCO, and XH<sub>2</sub>O by 94.0%,  
10 95.6%, 47.2%, and 96.8%, as shown in the third panel of Fig. 7. As CO absorbs weakly, the  
11 uncertainty in XCO is only reduced by 47.2%, which is significantly less than that for the other  
12 gases. The weak absorption of CO and the interferences from other strong absorbing gases such  
13 as CH<sub>4</sub> and H<sub>2</sub>O in the near-infrared are also noted by Buchwitz et al. (2004) and Galli et al.  
14 (2012). Our results corroborate Galli et al.'s findings that, due to interferences, the quality of the  
15 XCO retrieval is systematically influenced by the shortcomings in CH<sub>4</sub> and H<sub>2</sub>O spectroscopy.  
16 Nonetheless, the precisions for the simulated retrievals far exceed the measurement requirements  
17 discussed in Sec. 1, and thus leave a large margin for other sources of error such as uncertainty in  
18 the spectroscopic parameters.

19

20 We also notice that the precision and the UR of XCO retrievals tend to follow a diurnal pattern:  
21 precision is worse and UR lower at 12pm and 3pm than at 9am and 6pm. This might be due to  
22 the different light paths at different times of day. At 12pm and 3pm, the solar zenith angles are  
23 between 35° to 50°, so incoming sunlight travels through a relatively short path. In contrast, at  
24 9am and 6pm, the solar zenith angles are between 65° to 85°, so the sunlight traverses a longer  
25 light path in the atmosphere, resulting in stronger absorption signals and better precision. In other  
26 words, this diurnal pattern in precision might be a feature associated with the viewing geometry  
27 from geostationary orbit. Note that these results are based on a constant SNR of 300 and in real  
28 retrievals SNR could be kept constant at different times of day if the integration time is adjusted.  
29 Whether this diurnal pattern will persist in more simulated or real retrievals warrants more  
30 studies in the future.

31

### 1 **3.2 Influence of aerosols and clouds**

2 Aerosol and cloud contamination are substantial sources of systematic errors in trace gas  
3 retrievals (e.g., Dufour and Bréon, 2003; Houweling et al., 2005; Butz et al., 2011; O'Dell et al.,  
4 2012; Merrelli et al., 2015; Zhang et al., 2015). Novel cloud screening algorithms, such as the  
5 one designed for the OCO-2 mission, are able to screen out most of the scenes with thick clouds  
6 and aerosols. However, even after the pre-screening, some scenes are still contaminated with a  
7 small amount of aerosols and ice clouds that have a column-integrated OD less than  $\sim 0.30$   
8 (O'Dell et al., 2012). Following the study just mentioned, we also use OD less than  $\sim 0.30$  as the  
9 benchmark for a small amount of aerosols and ice clouds. In these cases, inaccurate retrievals of  
10 the optical properties of aerosols and ice clouds will negatively affect the quality of trace gas  
11 retrievals.

12

13 Here we briefly explore the influence of aerosols and ice clouds on trace gas retrievals and defer  
14 detailed investigations to later studies. We add realistic profiles of aerosols and ice clouds to the  
15 model atmosphere. It is assumed that the geometric and optical properties of aerosols and ice  
16 clouds are known with certainty. Scaling factors for aerosol OD and ice cloud OD are added to  
17 the state vector in Eq. (5) and retrievals are repeated for the test cases at 12pm, a time with larger  
18 radiance values and higher instrument noise than those at other times of day. Again, the a priori  
19 is 3% biased from the truth and has a 3% uncertainty. Compared to the clear-sky retrievals in  
20 Sec. 3.1, these retrievals are referred to as the all-sky retrievals. The sum of the aerosol and ice  
21 cloud ODs is the total particle OD.

22

23 Retrieving the ODs of aerosols and clouds from reflected sunlight in near-infrared bands, has  
24 been a significant challenge and an active area of scientific research (e.g., Reuter et al., 2010;  
25 Herbin et al., 2013). As there are now 11 elements in the state vector (9 elements in Eq. (5) and 2  
26 new elements added), the theoretical upper limit for DoF is 11. However, the real DoF is only  
27 about 10.2, mainly due to the lack of information to accurately retrieve the ODs of aerosols and  
28 clouds.

29

30 Figure 8 shows the retrieval biases, precisions, and URs of the four target species as a function of  
31 the total particle OD. Increases in the total particle OD lead to notable increases in the retrieval

1 biases of all four gases. For  $XCH_4$  and  $XH_2O$ , the average retrieval biases increase from  $< 0.4\%$   
2 for clear-sky retrievals to 1–3% for all-sky retrievals. For  $XCO_2$ , the biases increase from  $\sim 0.2\%$   
3 to  $\sim 0.5\%$ . For  $XCO$ , the biases increase from  $\sim 1.8\%$  to 2–6%. Previous studies have obtained  
4 similar results. For example, Vidot et al. (2009) conducted simulated retrievals of  $XCO_2$  over  
5 liquid water clouds with OCO-2's three spectral bands. They found that the presence of  
6 undetected thin cirrus clouds affect all retrieval parameters significantly. These results  
7 corroborate the findings of Vidot et al. (2009) that inaccurate retrievals of aerosol and cloud ODs  
8 cause substantial biases in  $XCO_2$  retrievals. Through simultaneous retrievals of all four gases, we  
9 find that aerosols and clouds cause biases not only in  $XCO_2$  retrievals, but also in all of the trace  
10 gas retrievals studied here. Generally, the higher the total particle OD, the worse the retrieval  
11 biases are. Spectral measurements from GeoFTS alone do not provide enough information about  
12 the optical properties of aerosols and cirrus clouds. This suggests that more effective pre-  
13 screening algorithms and better prior knowledge of the aerosol and cloud properties and/or  
14 vertical distributions are needed in order to mitigate biases caused by aerosols and clouds.

15  
16 There are two main causes behind the increase in the retrieval bias. One is the interference  
17 between absorption by gases and scattering by aerosols and clouds. The other one is the increase  
18 in the forward model error when the total particle OD increases. VLIDORT-16 stream is better at  
19 characterizing the multiple light scattering by aerosols and clouds, while 2S-ESS treats light  
20 scattering in a more approximate manner. This leads to an increase in the forward model error,  
21 and therefore, a corresponding increase in the retrieval bias. These results highlight the need for  
22 sophisticated radiative transfer models such as VLIDORT, along with better models to  
23 characterize the properties of aerosols and clouds and/or their vertical distributions, so that the  
24 forward model error can be minimized for real operational retrievals.

25  
26 In contrast, the single-measurement precision does not change much when the total particle OD  
27 changes. This is expected because, according to Eq. (8), the a posteriori uncertainty and the  
28 precision depend on  $S_a$ ,  $S_e$ , and  $K$  only. Changes in total particle OD only affect  $S_e$  and  $K$   
29 slightly, resulting in some minor worsening of the retrieval precision, as illustrated in Fig. 8.  
30 These results corroborate the findings of Kuang et al. (2002) using simulations. They also  
31 investigated the achievable  $XCO_2$  precisions as a function of the total particle OD and found that,



1 as OD increases from 0.05 to 0.25, the retrieval precision of XCO<sub>2</sub> over land only changes from  
2 ~0.5 ppm (~0.13%) to ~1.0 ppm (~0.26%). Our results show that the retrieval precisions of all  
3 four gases in the absolute sense are only slightly affected by the small amount of aerosol and  
4 cloud contamination. Thus, this study provides evidence that the single-measurement precisions  
5 for simulated clear-sky and all-sky retrievals meet measurement requirements for accurate flux  
6 inversions (Sec. 1).

### 7 8 **3.3 Choices of SNR and spectral resolution**

9 The previous sections present retrieval results when SNR and spectral resolution are set at 300  
10 and 0.25 cm<sup>-1</sup>, respectively. Optimal choices of SNR and spectral resolution can result in better  
11 cost-benefit ratio for a geostationary mission. Here we study the effect of varying SNR and  
12 spectral resolution on both clear-sky and all-sky retrievals. For simplicity, the two variables are  
13 assumed to be independent of each other. To allow easy comparison with retrieval results in Sec.  
14 3.1 and 3.2, the a priori values are same as before. Figure 9 shows the retrieval precision as a  
15 function of SNR and spectral resolution, which are set to vary from 50 to 250 and from 0.10 to  
16 0.30 cm<sup>-1</sup>, respectively. These ranges are chosen so as to cover some possible scenarios for real  
17 spaceborne measurements. The total particle OD is zero for clear-sky retrievals and 0.20 for all-  
18 sky retrievals. The results shown here are based on one test case at 12pm at Location 1. Other  
19 test cases exhibit similar patterns (not shown).

20  
21 For both clear-sky and all-sky retrievals, the retrieval precision is a strong function of both SNR  
22 and spectral resolution. Generally, it increases with higher SNR and finer spectral resolution.  
23 Comparing clear-sky and all-sky retrievals, we notice that the precisions for all trace gas  
24 retrievals are slightly worse in all-sky retrievals. This is a manifestation of the influence of  
25 aerosols and ice clouds, as discussed in Sec. 3.2. In particular, the XCO retrievals are more  
26 sensitive to changes in SNR and spectral resolution because of its weak absorption. It is clear  
27 that the quality of XCO retrievals is a significant function of both SNR and spectral resolution.  
28 The importance of XCO retrievals for surface flux inversions has been emphasized in Rayner et  
29 al. (2014). They investigated the ability of trace gas retrievals to constrain regional GHG  
30 emissions and found that XCO retrievals play the most important role in constraining urban  
31 emissions at 3 km resolution. Our results show that the choices of SNR and spectral resolution

1 will be of paramount importance for XCO retrievals. This exploratory study could help guide  
2 decisions on GeoFTS SNR and spectral resolution, which can result in cost-effective  
3 measurement strategies while achieving satisfactory levels of retrieval precisions.

#### 4 5 **4. Conclusion**

6  
7 This study explores the prospective performance of trace gas retrievals using simulated spectra  
8 measured by a Geostationary Fourier Transform Spectrometer (GeoFTS). The major scientific  
9 contributions of this study are as follows:

- 10
- 11 1) We have performed simulated retrievals over a significant range of atmospheric and surface  
12 scenarios in clear sky conditions over North America, one potential target for the GeoFTS.  
13 We find that, with no uncertainty in spectroscopy, the average retrieval biases and single-  
14 measurement precisions are  $< 0.2\%$  for XCO<sub>2</sub>, XCH<sub>4</sub>, and XH<sub>2</sub>O, and  $< 2\%$  for XCO. These  
15 results are based on a priori values with a bias of 3% and an uncertainty of 3%.
  - 16 2) We have briefly explored the influence of aerosols and ice clouds on trace gas retrievals. An  
17 increase in the amount of aerosols and ice clouds leads to a notable increase in the retrieval  
18 errors and slight worsening of the retrieval precisions. This study provides evidence that the  
19 single-measurement precisions for simulated clear-sky and all-sky retrievals meet the  
20 requirements for GeoFTS and leave a large margin for other sources of imprecisions in real  
21 retrievals.
  - 22 3) We have studied the effects of varying signal-to-noise ratio (SNR) and spectral resolution on  
23 both clear-sky and all-sky retrievals. We find that retrieval precision is a strong function of  
24 the two variables. This exploratory study can help guide decisions on GeoFTS SNR and  
25 spectral resolution, which can result in cost-effective measurement strategies while achieving  
26 satisfactory levels of retrieval precisions.

27  
28 While this study offers new scientific insights through simulated retrievals, it is worth pointing  
29 out that these numerical simulations often provide overoptimistic assessments of the capability of  
30 the observing system. This is partly because the instrument noise added to the synthetic data is  
31 random, which is unlikely to be the case for real measurements. Furthermore, uncertainty in the

- 1 spectroscopic parameters, imperfect aerosol/cloud filtering, and various instrument issues will
- 2 complicate real retrievals. Future studies will focus on how uncertainties in these factors affect
- 3 the retrieval results.

1 **Acknowledgements**

2

3 The authors would like to thank Renyu Hu, Pushkar Kopparla, Michael Wong, Le Kuai, Clare  
4 (Kam Weng) Wong, and Dejian Fu for helpful discussions. The authors also appreciate technical  
5 support from Michael Black and administrative support from Margaret Carlos and Irma Black.  
6 Valuable comments and suggestions from two reviewers are greatly appreciated. This research  
7 was supported in part by NASA grant NNX13AK34G to the California Institute of Technology,  
8 grant P1367828 from the Jet Propulsion Laboratory, and the KISS program at Caltech.

1 **References**

2

3 Aumann, H. H., Chahine, M. T., Gautier, C., Goldberg, M. D., Kalnay, E., McMillin, L. M.,  
4 Revercomb, H., Rosenkranz, P. W., Smith, W. L., Staelin, D. H., Strow, L. L. and Susskind, J.:  
5 AIRS/AMSU/HSB on the Aqua mission: Design, Science Objectives, Data Products, and  
6 Processing Systems, *IEEE Trans. Geosci. Remote Sens.*, 41(2), 253–264,  
7 doi:10.1109/TGRS.2002.808356, 2003.

8

9 Baker, D. F., Bösch, H., Doney, S. C., O’Brien, D. and Schimel, D. S.: Carbon source/sink  
10 information provided by column CO<sub>2</sub> measurements from the Orbiting Carbon Observatory,  
11 *Atmos. Chem. Phys.*, 10(9), 4145–4165, doi:10.5194/acp-10-4145-2010, 2010.

12

13 Bengtsson, L.: The global atmospheric water cycle, *Environ. Res. Lett.*, 5(2), 025202,  
14 doi:10.1088/1748-9326/5/2/025202, 2010.

15

16 Bey, I., Jacob, D. J., Yantosca, R. M., Logan, J. A., Field, B. D., Fiore, A. M., Li, Q., Liu, H. Y.,  
17 Mickley, L. J. and Schultz, M. G.: Global modeling of tropospheric chemistry with assimilated  
18 meteorology: Model description and evaluation, *J. Geophys. Res.*, 106(D19), 23073,  
19 doi:10.1029/2001JD000807, 2001.

20

21 Bréon, F., O’Brien, D. and Spinhirne, J.: Scattering layer statistics from space borne GLAS  
22 observations, *Geophys. Res. Lett.*, 32(22), L22802, doi:10.1029/2005GL023825, 2005.

23

24 Buchwitz, M., de Beek, R., Bramstedt, K., Noël, S., Bovensmann, H. and Burrows, J. P.: Global  
25 carbon monoxide as retrieved from SCIAMACHY by WFM-DOAS, *Atmos. Chem. Phys.*, 4(7),  
26 1945–1960, doi:10.5194/acp-4-1945-2004, 2004.

27

28 Buchwitz, M., Schneising, O., Burrows, J. P., Bovensmann, H., Reuter, M. and Notholt, J.: First  
29 direct observation of the atmospheric CO<sub>2</sub> year-to-year increase from space, *Atmos. Chem.*  
30 *Phys.*, 7(16), 4249–4256, doi:10.5194/acp-7-4249-2007, 2007.

31

1 Buchwitz, M., Reuter, M., Bovensmann, H., Pillai, D., Heymann, J., Schneising, O., Rozanov,  
2 V., Krings, T., Burrows, J. P., Boesch, H., Gerbig, C., Meijer, Y., and Löscher, A.: Carbon  
3 Monitoring Satellite (CarbonSat): assessment of atmospheric CO<sub>2</sub> and CH<sub>4</sub> retrieval errors by  
4 error parameterization, *Atmos. Meas. Tech.*, 6, 3477-3500, doi:10.5194/amt-6-3477-2013, 2013.  
5  
6 Butz, A., Guerlet, S., Hasekamp, O., Schepers, D., Galli, A., Aben, I., Frankenberg, C.,  
7 Hartmann, J.-M., Tran, H., Kuze, A., Keppel-Aleks, G., Toon, G., Wunch, D., Wennberg, P.,  
8 Deutscher, N., Griffith, D., Macatangay, R., Messerschmidt, J., Notholt, J. and Warneke, T.:  
9 Toward accurate CO<sub>2</sub> and CH<sub>4</sub> observations from GOSAT, *Geophys. Res. Lett.*, 38(14), L14812,  
10 doi:10.1029/2011GL047888, 2011.  
11  
12 Chahine, M., Barnett, C., Olsen, E. T., Chen, L. and Maddy, E.: On the determination of  
13 atmospheric minor gases by the method of vanishing partial derivatives with application to CO<sub>2</sub>,  
14 *Geophys. Res. Lett.*, 32(22), L22803, doi:10.1029/2005GL024165, 2005.  
15  
16 Chahine, M. T., Chen, L., Dimotakis, P., Jiang, X., Li, Q., Olsen, E. T., Pagano, T., Randerson, J.  
17 and Yung, Y. L.: Satellite remote sounding of mid-tropospheric CO<sub>2</sub>, *Geophys. Res. Lett.*,  
18 35(17), L17807, doi:10.1029/2008GL035022, 2008.  
19  
20 Chevallier, F., Engelen, R. J. and Peylin, P.: The contribution of AIRS data to the estimation of  
21 CO<sub>2</sub> sources and sinks, *Geophys. Res. Lett.*, 32(23), L23801, doi:10.1029/2005GL024229, 2005.  
22  
23 Clough, S. A., Shephard, M. W., Mlawer, E. J., Delamere, J. S., Iacono, M. J., Cady-Pereira, K.,  
24 Boukabara, S. and Brown, P. D.: Atmospheric radiative transfer modeling: a summary of the  
25 AER codes, *J. Quant. Spectrosc. Radiat. Transf.*, 91(2), 233–244,  
26 doi:10.1016/j.jqsrt.2004.05.058, 2005.  
27  
28 Crisp, D., Atlas, R. M., Breon, F.-M., Brown, L. R., Burrows, J. P., Ciais, P., Connor, B. J.,  
29 Doney, S. C., Fung, I. Y., Jacob, D. J., Miller, C. E., O'Brien, D., Pawson, S., Randerson, J. T.,  
30 Rayner, P., Salawitch, R. J., Sander, S. P., Sen, B., Stephens, G. L., Tans, P. P., Toon, G. C.,  
31 Wennberg, P. O., Wofsy, S. C., Yung, Y. L., Kuang, Z., Chudasama, B., Sprague, G., Weiss, B.,

1 Pollock, R., Kenyon, D. and Schroll, S.: The Orbiting Carbon Observatory (OCO) mission, *Adv.*  
2 *Sp. Res.*, 34(4), 700–709, doi:10.1016/j.asr.2003.08.062, 2004.

3

4 Crisp, D., Fisher, B. M., O’Dell, C., Frankenberg, C., Basilio, R., Bösch, H., Brown, L. R.,  
5 Castano, R., Connor, B., Deutscher, N. M., Eldering, A., Griffith, D., Gunson, M., Kuze, A.,  
6 Mandrake, L., McDuffie, J., Messerschmidt, J., Miller, C. E., Morino, I., Natraj, V., Notholt, J.,  
7 O’Brien, D. M., Oyafuso, F., Polonsky, I., Robinson, J., Salawitch, R., Sherlock, V., Smyth, M.,  
8 Suto, H., Taylor, T. E., Thompson, D. R., Wennberg, P. O., Wunch, D. and Yung, Y. L.: The  
9 ACOS CO<sub>2</sub> retrieval algorithm – Part II: Global XCO<sub>2</sub> data characterization, *Atmos. Meas.*  
10 *Tech.*, 5(4), 687–707, doi:10.5194/amt-5-687-2012, 2012.

11

12 Connor, B. J., Boesch, H., Toon, G., Sen, B., Miller, C. and Crisp, D.: Orbiting Carbon  
13 Observatory: Inverse method and prospective error analysis, *J. Geophys. Res. Atmos.*, 113(D5),  
14 D05305, doi:10.1029/2006JD008336, 2008.

15

16 Dufour, E. and Bréon, F.-M.: Spaceborne Estimate of Atmospheric CO<sub>2</sub> Column by Use of the  
17 Differential Absorption Method: Error Analysis, *Appl. Opt.*, 42(18), 3595,  
18 doi:10.1364/AO.42.003595, 2003.

19

20 Fu, D., Pongetti, T. J., Blavier, J. F. L., Crawford, T. J., Manatt, K. S., Toon, G. C., Wong, K.  
21 W., and Sander, S. P.: Near-infrared remote sensing of Los Angeles trace gas distributions from  
22 a mountaintop site, *Atmos. Meas. Tech.*, 7, 713-729, doi:10.5194/amt-7-713-2014, 2014.

23

24 Galli, A., Butz, A., Scheepmaker, R. A., Hasekamp, O., Landgraf, J., Tol, P., Wunch, D.,  
25 Deutscher, N. M., Toon, G. C., Wennberg, P. O., Griffith, D. W. T., and Aben, I.: CH<sub>4</sub>, CO, and  
26 H<sub>2</sub>O spectroscopy for the Sentinel-5 Precursor mission: an assessment with the Total Carbon  
27 Column Observing Network measurements, *Atmos. Meas. Tech.*, 5, 1387-1398, 10.5194/amt-5-  
28 1387-2012, 2012.

29

1 Herbin, H., Labonnote, L. C. and Dubuisson, P.: Multispectral information from TANSO-FTS  
2 instrument – Part 2: Application to aerosol effect on greenhouse gas retrievals, *Atmos. Meas.*  
3 *Tech.*, 6(11), 3313–3323, doi:10.5194/amt-6-3313-2013, 2013.

4

5 Heymsfield, A., Bansemer, A., Field, P., Durden, S., Stith, J., Dye, J., Hall, W. and Grainger, C.:  
6 Observations and Parameterizations of Particle Size Distributions in Deep Tropical Cirrus and  
7 Stratiform Precipitating Clouds: Results from In Situ Observations in TRMM Field Campaigns,  
8 *Journal of the Atmospheric Sciences*, 59(24), 3457–3491, doi:10.1175/1520-0469(2002)059,  
9 2002.

10

11 Houghton, R. A.: Balancing the Global Carbon Budget, *Annu. Rev. Earth Planet. Sci.*, 35(1),  
12 313–347, doi:10.1146/annurev.earth.35.031306.140057, 2007.

13

14 Houweling, S., Hartmann, W., Aben, I., Schrijver, H., Skidmore, J., Roelofs, G.-J. and Breon, F.-  
15 M.: Evidence of systematic errors in SCIAMACHY-observed CO<sub>2</sub> due to aerosols, *Atmos.*  
16 *Chem. Phys.*, 5, 3003–3013, doi:10.5194/acp-5-3003-2005, 2005.

17

18 Hungershofer, K., Breon, F.-M., Peylin, P., Chevallier, F., Rayner, P., Klonecki, A., Houweling,  
19 S. and Marshall, J.: Evaluation of various observing systems for the global monitoring of CO<sub>2</sub>  
20 surface fluxes, *Atmos. Chem. Phys.*, 10(21), 10503–10520, doi:10.5194/acp-10-10503-2010,  
21 2010.

22

23 IPCC: Climate Change 2013: The physical science basis. Contribution of working group I to the  
24 fifth assessment report of the Intergovernmental Panel on Climate Change, edited by: Stocker, T.  
25 F., Qin, D., Plattner, G.-K., Tignor, M., Allen, S. K., Boschung, J., Nauels, A., Xia, Y., Bex, V.,  
26 and Midgley, P. M., Cambridge University Press, Cambridge, United Kingdom and New York,  
27 NY, USA, 1535 pp., 2013.

28

29 Jacob, F., Petitcolin, F., Schmugge, T., Vermote, É., French, A. and Ogawa, K.: Comparison of  
30 land surface emissivity and radiometric temperature derived from MODIS and ASTER sensors,  
31 *Remote Sens. Environ.*, 90(2), 137–152, doi:10.1016/j.rse.2003.11.015, 2004.



1  
2 Key, R., Sander, S., Eldering, A., Miller, C., Frankenberg, C., Natraj, V., Rider, D., Blavier, J.,  
3 Bekker, D. and Wu, Y. H.: The Geostationary Carbon Process Mapper, in 2012 IEEE Aerospace  
4 Conference, pp. 1–16, IEEE., 2012.  
5  
6 Kuai, L., Natraj, V., Shia, R.-L., Miller, C. and Yung, Y. L.: Channel selection using information  
7 content analysis: A case study of CO<sub>2</sub> retrieval from near infrared measurements, *J. Quant.*  
8 *Spectrosc. Radiat. Transf.*, 111(9), 1296–1304, doi:10.1016/j.jqsrt.2010.02.011, 2010.  
9  
10 Kuang, Z., Margolis, J., Toon, G., Crisp, D. and Yung, Y.: Spaceborne measurements of  
11 atmospheric CO<sub>2</sub> by high-resolution NIR spectrometry of reflected sunlight: An introductory  
12 study, *Geophys. Res. Lett.*, 29(15), 11–1–11–4, doi:10.1029/2001GL014298, 2002.  
13  
14 Le Quéré, C., Raupach, M. R., Canadell, J. G., Marland, G., Bopp, L., Ciais, P., Conway, T. J.,  
15 Doney, S. C., Feely, R. A., Foster, P., Friedlingstein, P., Gurney, K., Houghton, R. A., House, J.  
16 I., Huntingford, C., Levy, P. E., Lomas, M. R., Majkut, J., Metzl, N., Ometto, J. P., Peters, G. P.,  
17 Prentice, I. C., Randerson, J. T., Running, S. W., Sarmiento, J. L., Schuster, U., Sitch, S.,  
18 Takahashi, T., Viovy, N., van der Werf, G. R. and Woodward, F. I.: Trends in the sources and  
19 sinks of carbon dioxide, *Nat. Geosci.*, 2(12), 831–836, doi:10.1038/ngeo689, 2009.  
20  
21 Le Quéré, C., Peters, G. P., Andres, R. J., Andrew, R. M., Boden, T. A., Ciais, P., Friedlingstein,  
22 P., Houghton, R. A., Marland, G., Moriarty, R., Sitch, S., Tans, P., Arneeth, A., Arvanitis, A.,  
23 Bakker, D. C. E., Bopp, L., Canadell, J. G., Chini, L. P., Doney, S. C., Harper, A., Harris, I.,  
24 House, J. I., Jain, A. K., Jones, S. D., Kato, E., Keeling, R. F., Klein Goldewijk, K., Körtzinger,  
25 A., Koven, C., Lefèvre, N., Maignan, F., Omar, A., Ono, T., Park, G. H., Pfeil, B., Poulter, B.,  
26 Raupach, M. R., Regnier, P., Rödenbeck, C., Saito, S., Schwinger, J., Segschneider, J., Stocker,  
27 B. D., Takahashi, T., Tilbrook, B., van Heuven, S., Viovy, N., Wanninkhof, R., Wiltshire, A.,  
28 and Zaehle, S.: Global carbon budget 2013, *Earth Syst. Sci. Data*, 6, 235-263, 10.5194/essd-6-  
29 235-2014, 2014.  
30

1 Levenberg, K.: A method for the solution of certain problems in least squares, *Quart. Applied*  
2 *Math.*, 2, 164-168, 1944.  
3  
4 Marquardt, D. W.: An Algorithm for Least-Squares Estimation of Nonlinear Parameters, *J. Soc.*  
5 *Indust. Appl. Math.*, 11(2), 431-441, 10.1137/0111030, 1963.  
6  
7 Merrelli, A., Bennartz, R., O'Dell, C. W. and Taylor, T. E.: Estimating bias in the OCO-2  
8 retrieval algorithm caused by 3-D radiation scattering from unresolved boundary layer clouds,  
9 *Atmos. Meas. Tech.*, 8(4), 1641–1656, doi:10.5194/amt-8-1641-2015, 2015.  
10  
11 Nassar, R., Jones, D. B. A., Kulawik, S. S., Worden, J. R., Bowman, K. W., Andres, R. J.,  
12 Suntharalingam, P., Chen, J. M., Brenninkmeijer, C. A. M., Schuck, T. J., Conway, T. J., and  
13 Worthy, D. E.: Inverse modeling of CO<sub>2</sub> sources and sinks using satellite observations of CO<sub>2</sub>  
14 from TES and surface flask measurements, *Atmos. Chem. Phys.*, 11, 6029-6047,  
15 doi:10.5194/acp-11-6029-2011, 2011.  
16  
17 Natraj, V.: A review of fast radiative transfer techniques, in *Light Scattering Reviews 8*, edited  
18 by A. A. Kokhanovsky, pp. 475–504, Springer Berlin Heidelberg, Berlin, Heidelberg., 2013.  
19  
20 Newman, S., Jeong, S., Fischer, M. L., Xu, X., Haman, C. L., Lefer, B., Alvarez, S.,  
21 Rappenglueck, B., Kort, E. A., Andrews, A. E., Peischl, J., Gurney, K. R., Miller, C. E. and  
22 Yung, Y. L.: Diurnal tracking of anthropogenic CO<sub>2</sub> emissions in the Los Angeles basin  
23 megacity during spring 2010, *Atmos. Chem. Phys.*, 13(8), 4359–4372, doi:10.5194/acp-13-4359-  
24 2013, 2013.  
25  
26 O'Dell, C. W., Connor, B., Bösch, H., O'Brien, D., Frankenberg, C., Castano, R., Christi, M.,  
27 Eldering, D., Fisher, B., Gunson, M., McDuffie, J., Miller, C. E., Natraj, V., Oyafuso, F.,  
28 Polonsky, I., Smyth, M., Taylor, T., Toon, G. C., Wennberg, P. O. and Wunch, D.: The ACOS  
29 CO<sub>2</sub> retrieval algorithm – Part 1: Description and validation against synthetic observations,  
30 *Atmos. Meas. Tech.*, 5(1), 99–121, doi:10.5194/amt-5-99-2012, 2012.  
31

1 Polonsky, I. N., O'Brien, D. M., Kumer, J. B. and O'Dell, C. W.: Performance of a geostationary  
2 mission, geoCARB, to measure CO<sub>2</sub>, CH<sub>4</sub> and CO column-averaged concentrations, *Atmos.*  
3 *Meas. Tech.*, 7(4), 959–981, doi:10.5194/amt-7-959-2014, 2014.

4

5 Rayner, P. J. and O'Brien, D. M.: The utility of remotely sensed CO<sub>2</sub> concentration data in  
6 surface source inversions, *Geophys. Res. Lett.*, 28(1), 175–178, doi:10.1029/2000GL011912,  
7 2001.

8

9 Rayner, P. J., Utembe, S. R. and Crowell, S.: Constraining regional greenhouse gas emissions  
10 using geostationary concentration measurements: a theoretical study, *Atmos. Meas. Tech.*, 7(10),  
11 3285–3293, doi:10.5194/amt-7-3285-2014, 2014.

12

13 Reuter, M., Buchwitz, M., Schneising, O., Heymann, J., Bovensmann, H. and Burrows, J. P.: A  
14 method for improved SCIAMACHY CO<sub>2</sub> retrieval in the presence of optically thin clouds,  
15 *Atmos. Meas. Tech.*, 3(1), 209–232, doi:10.5194/amt-3-209-2010, 2010.

16

17 Rodgers, C. D.: Information content and optimisation of high spectral resolution remote  
18 measurements, *Adv. Sp. Res.*, 21(3), 361–367, doi:10.1016/S0273-1177(97)00915-0, 1998.

19

20 Rodgers, C. D.: *Inverse Methods for Atmospheric Sounding: Theory and Practice*, World  
21 Scientific, Singapore, 2000.

22

23 Rothman, L. S., Gordon, I. E., Barbe, A., Benner, D. C., Bernath, P. F., Birk, M., Boudon, V.,  
24 Brown, L. R., Campargue, A., Champion, J.-P., Chance, K., Coudert, L. H., Dana, V., Devi, V.  
25 M., Fally, S., Flaud, J.-M., Gamache, R. R., Goldman, A., Jacquemart, D., Kleiner, I., Lacombe,  
26 N., Lafferty, W. J., Mandin, J.-Y., Massie, S. T., Mikhailenko, S. N., Miller, C. E., Moazzen-  
27 Ahmadi, N., Naumenko, O. V., Nikitin, A. V., Orphal, J., Perevalov, V. I., Perrin, A., Predoi-  
28 Cross, A., Rinsland, C. P., Rotger, M., Šimečková, M., Smith, M. A. H., Sung, K., Tashkun, S.  
29 A., Tennyson, J., Toth, R. A., Vandaele, A. C. and Vander Auwera, J.: The HITRAN 2008  
30 molecular spectroscopic database, *J. Quant. Spectrosc. Radiat. Transf.*, 110(9-10), 533–572,  
31 doi:10.1016/j.jqsrt.2009.02.013, 2009.

1  
2 Schimel, D. S., House, J. I., Hibbard, K. A., Bousquet, P., Ciais, P., Peylin, P., Braswell, B. H.,  
3 Apps, M. J., Baker, D., Bondeau, A., Canadell, J., Churkina, G., Cramer, W., Denning, A. S.,  
4 Field, C. B., Friedlingstein, P., Goodale, C., Heimann, M., Houghton, R. A., Melillo, J. M.,  
5 Moore III, B., Murdiyarso, D., Noble, I., Pacala, S. W., Prentice, I. C., Raupach, M. R., Rayner,  
6 P. J., Scholes, R. J., Steffen, W. L. and Wirth, C.: Recent patterns and mechanisms of carbon  
7 exchange by terrestrial ecosystems, *Nature*, 414(November), 169–172, 2001.

8  
9 Schneising, O., Buchwitz, M., Reuter, M., Heymann, J., Bovensmann, H. and Burrows, J. P.:  
10 Long-term analysis of carbon dioxide and methane column-averaged mole fractions retrieved  
11 from SCIAMACHY, *Atmos. Chem. Phys.*, 11(6), 2863–2880, doi:10.5194/acp-11-2863-2011,  
12 2011.

13  
14 Schrijver, H., Gloudemans, A. M. S., Frankenberg, C. and Aben, I.: Water vapour total columns  
15 from SCIAMACHY spectra in the 2.36  $\mu\text{m}$  window, *Atmos. Meas. Tech.*, 2(2), 561–571,  
16 doi:10.5194/amt-2-561-2009, 2009.

17  
18 Spurr, R. J. D.: VLIDORT: A linearized pseudo-spherical vector discrete ordinate radiative  
19 transfer code for forward model and retrieval studies in multilayer multiple scattering media, *J.*  
20 *Quant. Spectrosc. Radiat. Transf.*, 102(2), 316–342, doi:10.1016/j.jqsrt.2006.05.005, 2006.

21  
22 Spurr, R. and Natraj, V.: A linearized two-stream radiative transfer code for fast approximation  
23 of multiple-scatter fields, *J. Quant. Spectrosc. Radiat. Transf.*, 112(16), 2630–2637,  
24 doi:10.1016/j.jqsrt.2011.06.014, 2011.

25  
26 Vidot, J., Bennartz, R., O’Dell, C. W., Preusker, R., Lindstrot, R. and Heidinger, A. K.: CO<sub>2</sub>  
27 Retrieval over Clouds from the OCO Mission: Model Simulations and Error Analysis, *J. Atmos.*  
28 *Ocean. Technol.*, 26(6), 1090–1104, doi:10.1175/2009JTECHA1200.1, 2009.

29  
30 Wecht, K. J., Jacob, D. J., Sulprizio, M. P., Santoni, G. W., Wofsy, S. C., Parker, R., Bösch, H.  
31 and Worden, J.: Spatially resolving methane emissions in California: constraints from the

1 CalNex aircraft campaign and from present (GOSAT, TES) and future (TROPOMI,  
2 geostationary) satellite observations, *Atmos. Chem. Phys.*, 14(15), 8173–8184, doi:10.5194/acp-  
3 14-8173-2014, 2014.

4

5 Winker, D. M., Pelon, J., Coakley, J. A., Ackerman, S. A., Charlson, R. J., Colarco, P. R.,  
6 Flamant, P., Fu, Q., Hoff, R. M., Kittaka, C., Kubar, T. L., Le Treut, H., McCormick, M. P.,  
7 Mégie, G., Poole, L., Powell, K., Trepte, C., Vaughan, M. A. and Wielicki, B. A.: The Calipso  
8 Mission: A Global 3D View of Aerosols and Clouds, *Bull. Am. Meteorol. Soc.*, 91(September),  
9 1211–1229, doi:10.1175/2010BAMS3009.1, 2010.

10

11 Wong, K. W., Fu, D., Pongetti, T. J., Newman, S., Kort, E. A., Duren, R., Hsu, Y.-K., Miller, C.  
12 E., Yung, Y. L. and Sander, S. P.: Mapping CH<sub>4</sub> : CO<sub>2</sub> ratios in Los Angeles with CLARS-FTS  
13 from Mount Wilson, California, *Atmos. Chem. Phys.*, 15(1), 241–252, doi:10.5194/acp-15-241-  
14 2015, 2015.

15

16 Woods, T. N., Chamberlin, P. C., Harder, J. W., Hock, R. A., Snow, M., Eparvier, F. G.,  
17 Fontenla, J., McClintock, W. E. and Richard, E. C.: Solar Irradiance Reference Spectra (SIRS)  
18 for the 2008 Whole Heliosphere Interval (WHI), *Geophys. Res. Lett.*, 36(1), L01101,  
19 doi:10.1029/2008GL036373, 2009.

20

21 Wu, L., Bocquet, M., Lauvaux, T., Chevallier, F., Rayner, P., and Davis, K.: Optimal  
22 representation of source-sink fluxes for mesoscale carbon dioxide inversion with synthetic data,  
23 *Journal of Geophysical Research: Atmospheres*, 116, D21304, 10.1029/2011JD016198, 2011.

24

25 Wunch, D., Wennberg, P. O., Toon, G. C., Connor, B. J., Fisher, B., Osterman, G. B.,  
26 Frankenberg, C., Mandrake, L., O'Dell, C., Ahonen, P., Biraud, S. C., Castano, R., Cressie, N.,  
27 Crisp, D., Deutscher, N. M., Eldering, A., Fisher, M. L., Griffith, D. W. T., Gunson, M.,  
28 Heikkinen, P., Keppel-Aleks, G., Kyrö, E., Lindenmaier, R., Macatangay, R., Mendonca, J.,  
29 Messerschmidt, J., Miller, C. E., Morino, I., Notholt, J., Oyafuso, F. A., Rettinger, M., Robinson,  
30 J., Roehl, C. M., Salawitch, R. J., Sherlock, V., Strong, K., Susmann, R., Tanaka, T.,  
31 Thompson, D. R., Uchino, O., Warneke, T. and Wofsy, S. C.: A method for evaluating bias in

1 global measurements of CO<sub>2</sub> total columns from space, *Atmos. Chem. Phys.*, 11, 12317–12337,  
2 doi:10.5194/acp-11-12317-2011, 2011.

3

4 Xiong, X., Barnet, C., Maddy, E., Sweeney, C., Liu, X., Zhou, L. and Goldberg, M.:  
5 Characterization and validation of methane products from the Atmospheric Infrared Sounder  
6 (AIRS), *J. Geophys. Res.*, 113(G3), G00A01, doi:10.1029/2007JG000500, 2008.

7

8 Yokota, T., Yoshida, Y., Eguchi, N., Ota, Y., Tanaka, T., Watanabe, H., and Maksyutov, S.:  
9 Global Concentrations of CO<sub>2</sub> and CH<sub>4</sub> Retrieved from GOSAT: First Preliminary Results,  
10 *SOLA*, 5, 160-163, 10.2151/sola.2009-041, 2009.

11

12 Yoshida, Y., Ota, Y., Eguchi, N., Kikuchi, N., Nobuta, K., Tran, H., Morino, I., and Yokota, T.:  
13 Retrieval algorithm for CO<sub>2</sub> and CH<sub>4</sub> column abundances from short-wavelength infrared  
14 spectral observations by the Greenhouse gases observing satellite, *Atmos. Meas. Tech.*, 4, 717-  
15 734, 10.5194/amt-4-717-2011, 2011.

16

17 Zhang, Q., Natraj, V., Li, K., Shia, R., Fu, D., Pongetti, T., Sander, S. P., and Yung, Y. L.:  
18 Influence of aerosol scattering on the retrieval of CO<sub>2</sub> mixing ratios: a case study using  
19 measurements from the California Laboratory for Atmospheric Remote Sensing (CLARS), *J.*  
20 *Geophys. Res.-Atmos.*, accepted, 2015.

1 **Tables**

2

3 **Table 1.** The GeoFTS spectral bands and the target species.

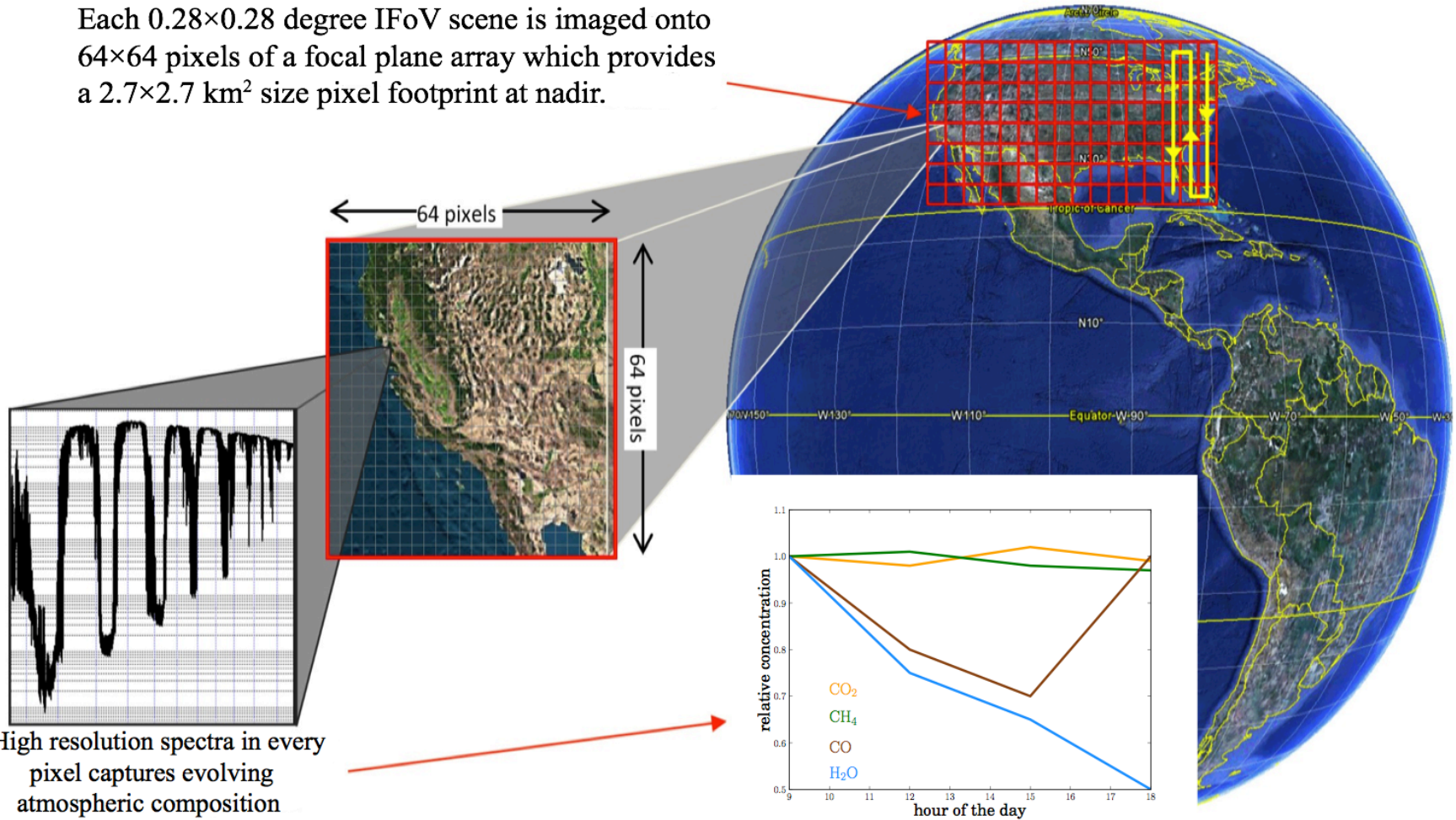
Band Number	Spectral Band	Target Species
1A	2.3 $\mu\text{m}$ (4210–4320 $\text{cm}^{-1}$ )	CH <sub>4</sub> , CO, H <sub>2</sub> O
1B	1.6 $\mu\text{m}$ (5950–6100 $\text{cm}^{-1}$ and 6190–6260 $\text{cm}^{-1}$ )	CH <sub>4</sub> , CO <sub>2</sub> , H <sub>2</sub> O
2	0.76 $\mu\text{m}$ (13000–13170 $\text{cm}^{-1}$ )	O <sub>2</sub>

4

1 **Figures**

2

Each  $0.28 \times 0.28$  degree IFOV scene is imaged onto  $64 \times 64$  pixels of a focal plane array which provides a  $2.7 \times 2.7$  km<sup>2</sup> size pixel footprint at nadir.



3

4

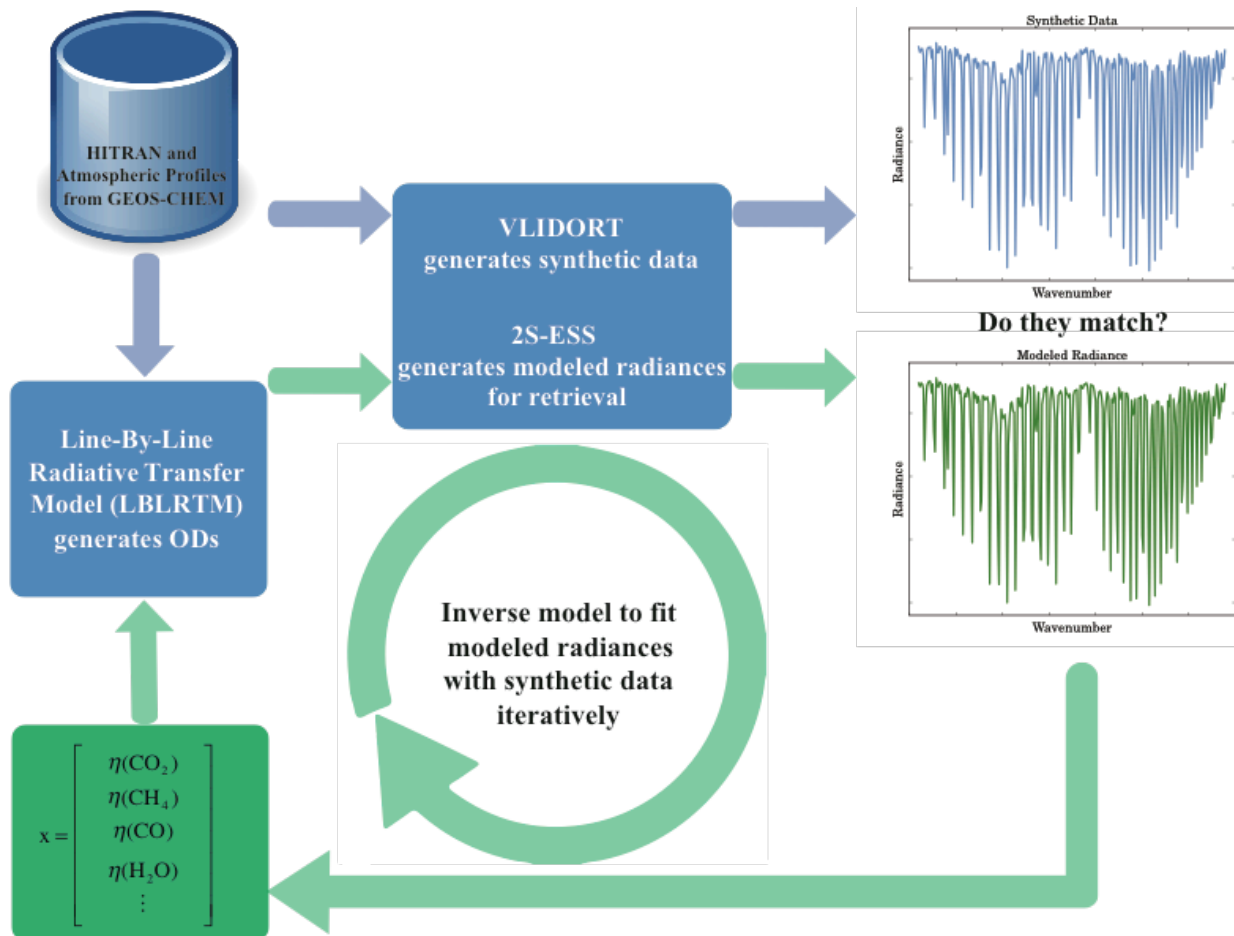
5

6

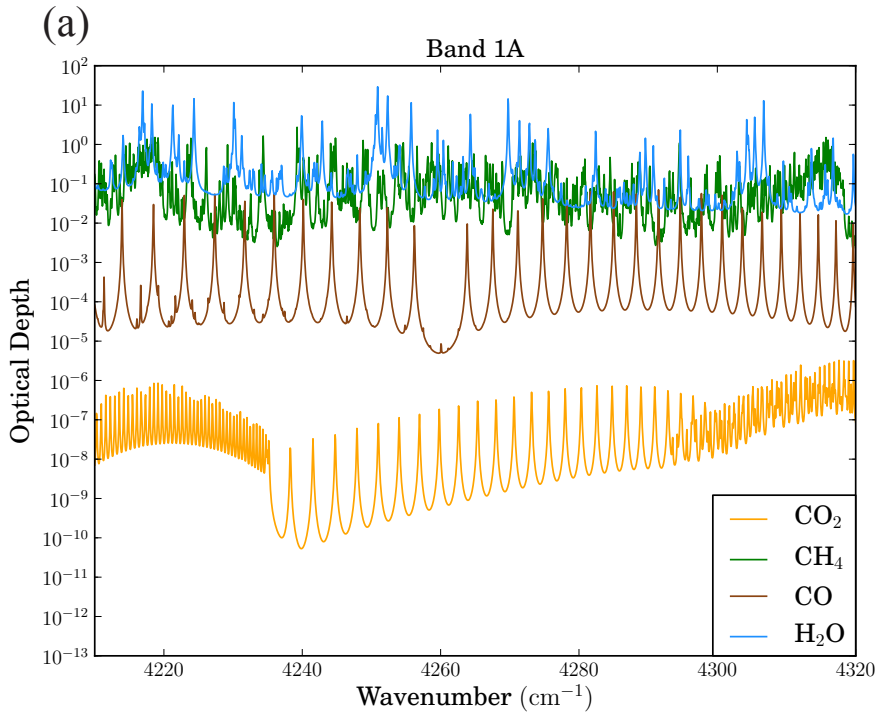
7

**Figure 1.** A schematic illustrating the GeoFTS observing system. Each  $0.28 \times 0.28$  degree Instantaneous Field of View (IFOV) scene is imaged onto  $64 \times 64$  pixels of a focal plane array, which provides a  $2.7 \times 2.7$  km<sup>2</sup> size pixel footprint at nadir. The evolving atmospheric compositions at different times of day are then inferred from the high-resolution spectra measured by the instrument. The relative concentrations of four target species with respect to those at 9am are shown for illustration purposes only.

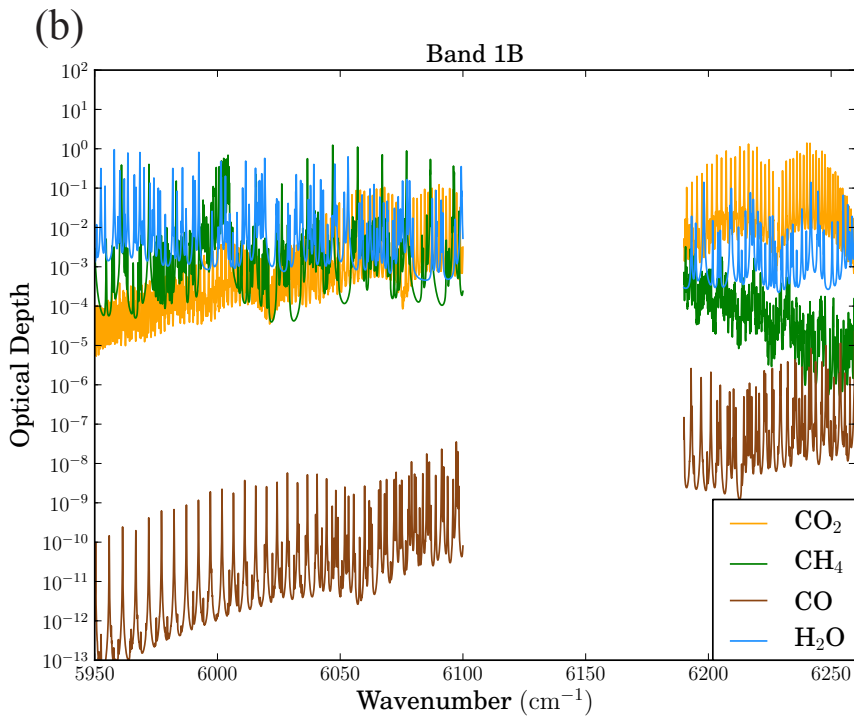




1  
 2 **Figure 2.** The set-up for simulated retrievals. Realistic atmospheric profiles are obtained from GEOS-CHEM and line positions and  
 3 strengths from the HITRAN 2008 molecular spectroscopic database. These are then input to a Line-By-Line Radiative Transfer Model  
 4 (LBLRTM) to generate optical depths. VLIDORT, a state-of-the-art radiative transfer model, generates the synthetic data after its  
 5 model output is convolved with the instrument line shape (ILS) and random measurement noise is added. A fast two-stream (2S),  
 6 enhanced single scattering (ESS) radiative transfer model, 2S-ESS, generates the modeled radiances for retrievals. In simulated  
 7 retrievals, we first have some prior knowledge about the concentration of gases and other parameters. This a priori is used as input to  
 8 2S-ESS to generate the modeled radiances. The state vector  $x$  is updated iteratively in an inverse model until the modeled radiances  
 9 match the synthetic data adequately.



1



2

3 **Figure 3.** The optical depths of four target species in the GeoFTS spectral bands: (a) for Band  
 4 1A and (b) for Band 1B. Band 1A is for retrievals of  $\text{CH}_4$ ,  $\text{CO}$ , and  $\text{H}_2\text{O}$ . Band 1B is for  
 5 retrievals of  $\text{CH}_4$ ,  $\text{CO}_2$ , and  $\text{H}_2\text{O}$ .

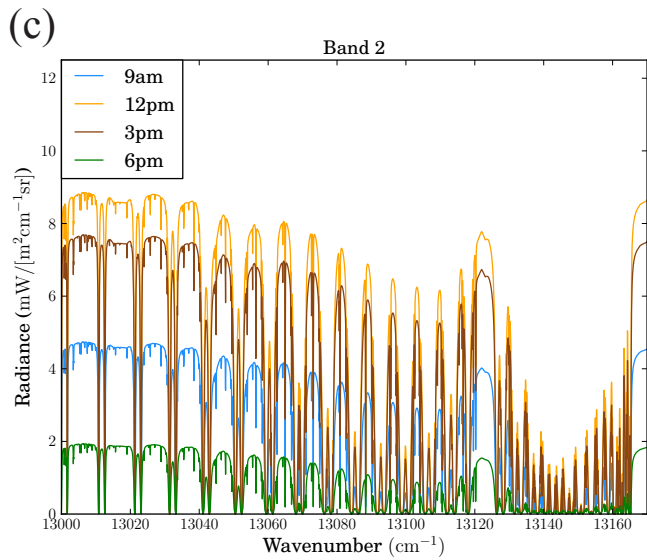
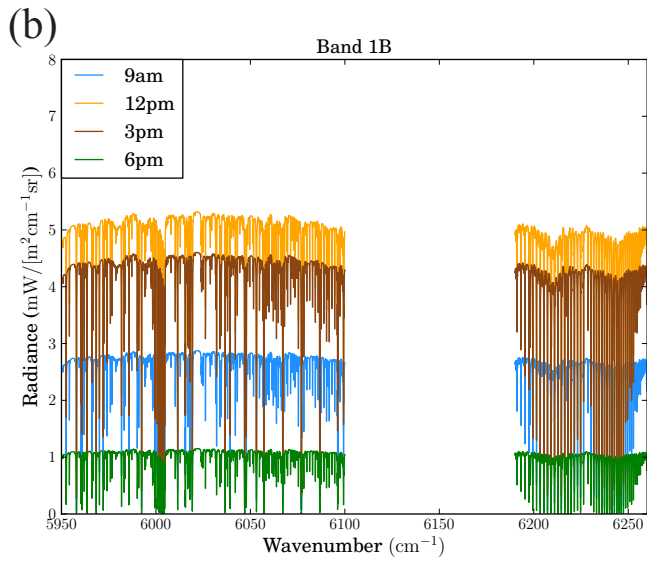
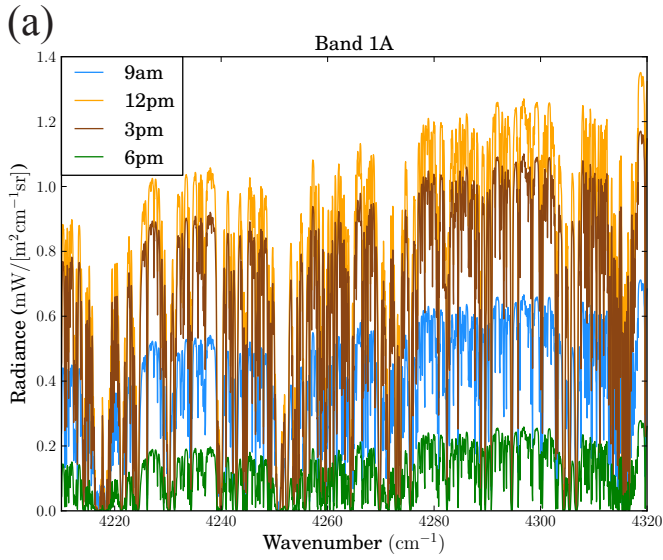


**Figure 4.** Modeled radiances in three spectral bands at four times of day at Location 1 on 26 July 2006.

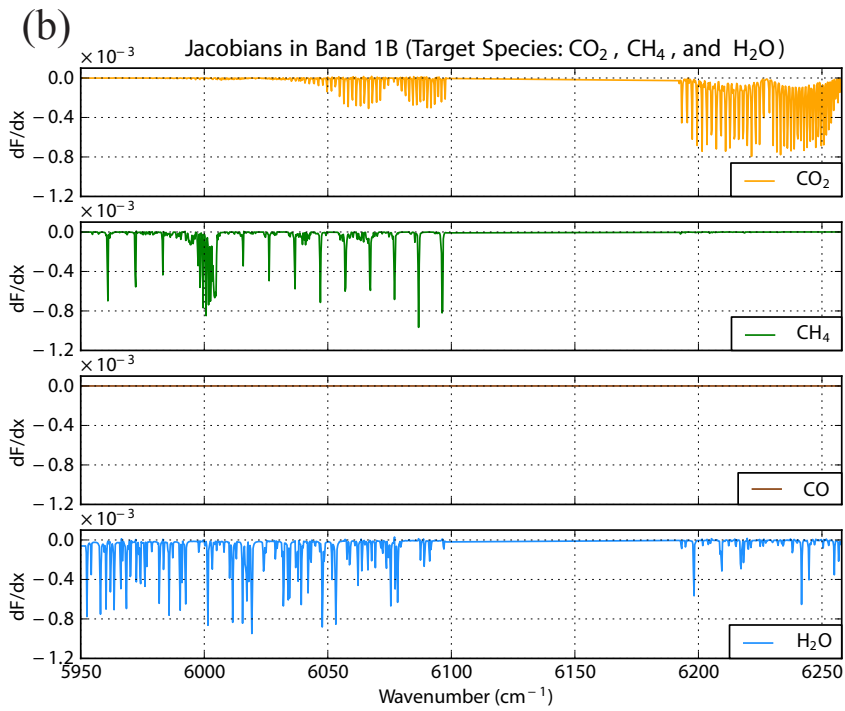
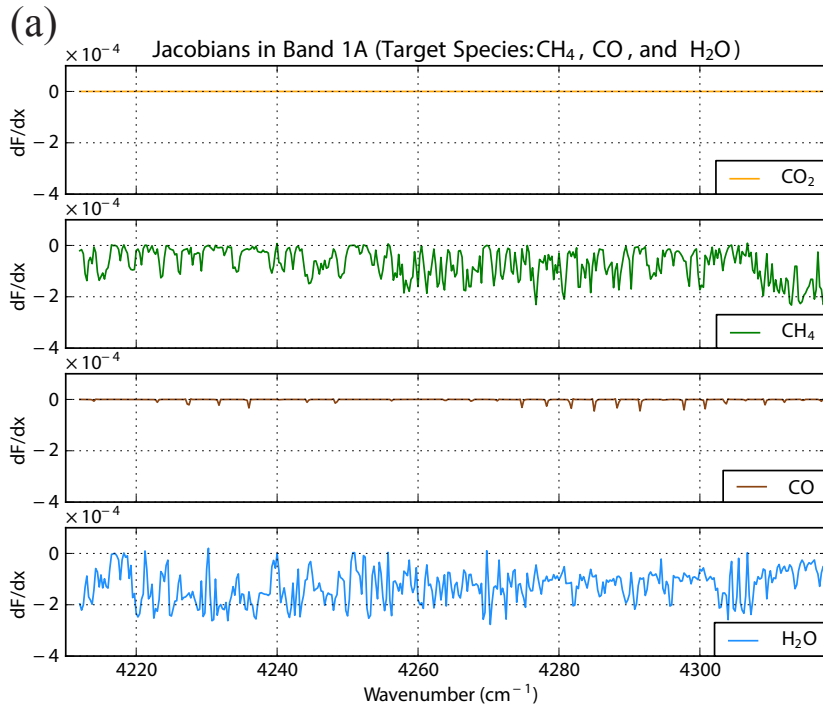
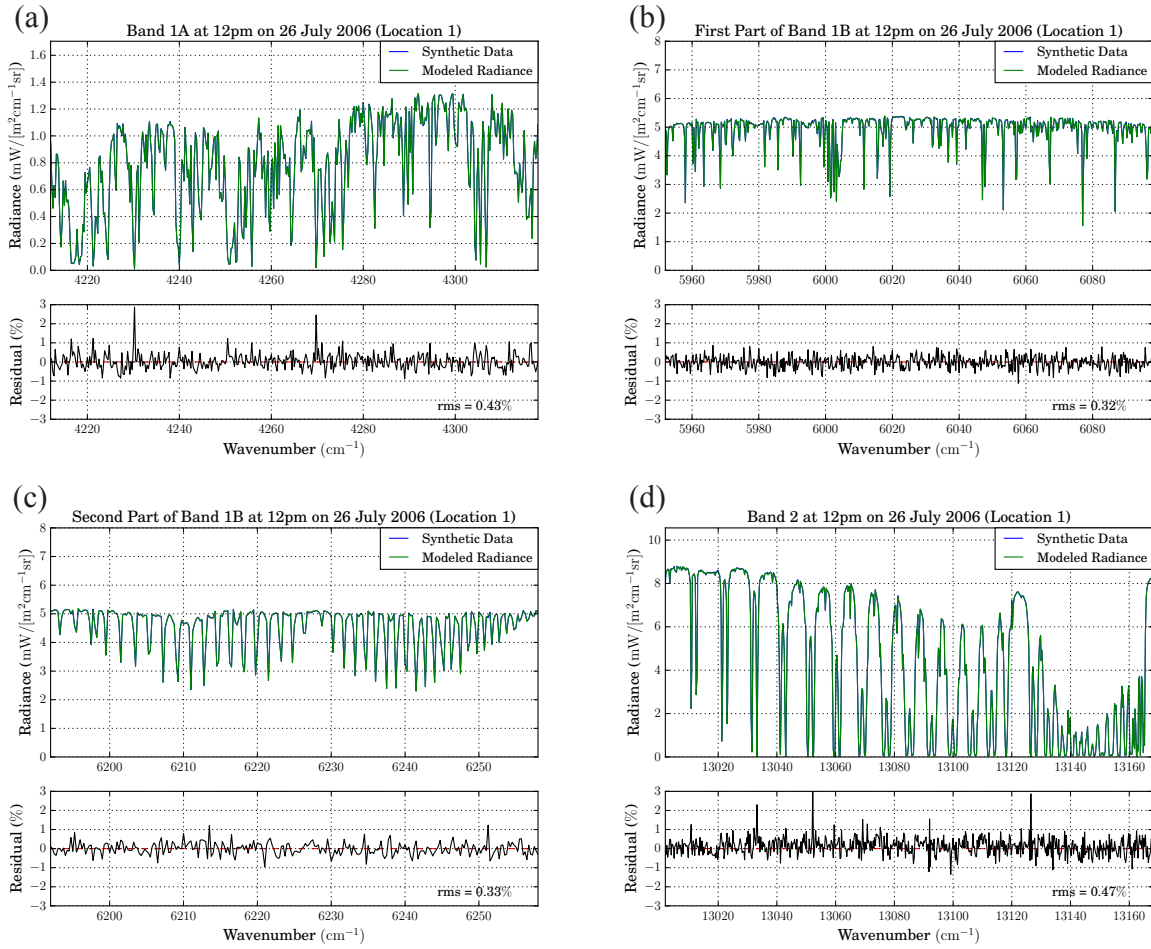
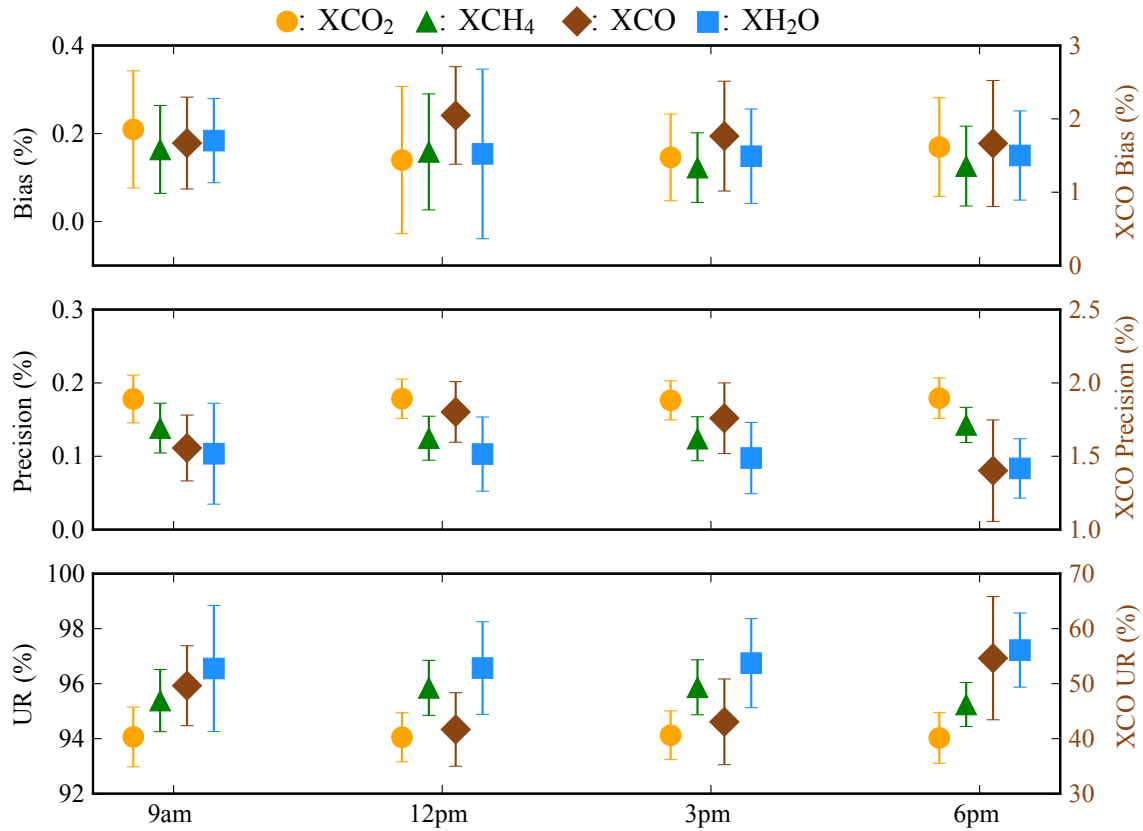


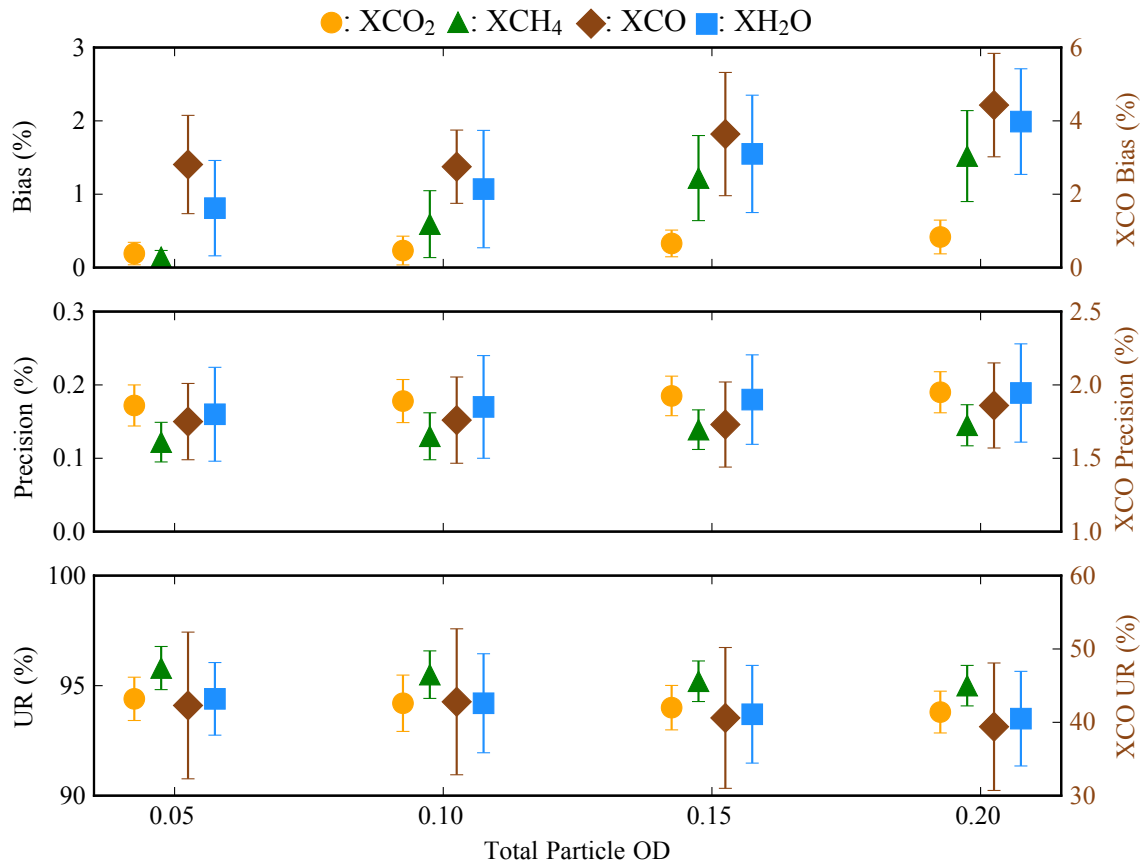
**Figure 5.** The Jacobians of four target species in (a) Band 1A and (b) Band 1B. Since  $x$  is a unitless scaling factor, the Jacobian ( $dF/dx$ ) has the same unit as the modeled radiances in Fig. 4.



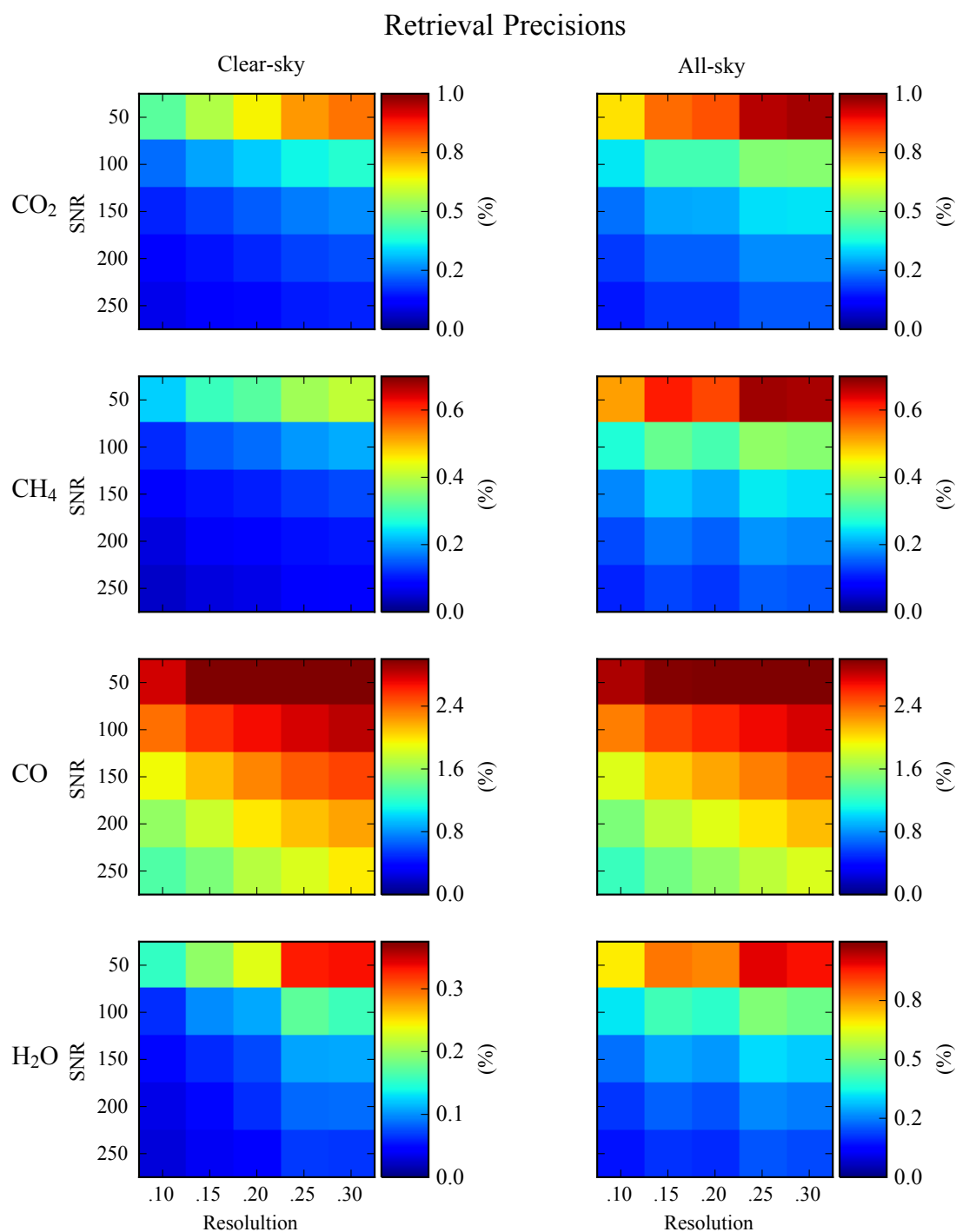
1  
 2 **Figure 6.** A sample spectral fit and residuals from a simulated clear-sky retrieval on 26 July  
 3 2006 at Location 1. The root-mean-square (rms) values of the residuals are between 0.32% and  
 4 0.47%.



1  
2 **Figure 7.** Average retrieval biases, precisions, and uncertainty reductions (UR) for simulated  
3 clear-sky retrievals at different times of day. SNR is 300 and spectral resolution is  $0.25 \text{ cm}^{-1}$ . The  
4 a priori is biased 3% from the truth and has a 3% uncertainty. The error bars are the standard  
5 deviations of retrieval results from all the test cases. Note that the scales for XCO<sub>2</sub>, XCH<sub>4</sub>, and  
6 XH<sub>2</sub>O are on the left-hand side whereas those for XCO are on the right-hand side.



1  
 2 **Figure 8.** Average retrieval biases, precisions, and uncertainty reductions (UR) for simulated all-  
 3 sky retrievals as a function of the total particle optical depth (OD). SNR is 300 and spectral  
 4 resolution is  $0.25 \text{ cm}^{-1}$ . The a priori is biased 3% from the truth and has a 3% uncertainty. The  
 5 error bars are the standard deviations of retrieval results from the test cases.



1  
 2 **Figure 9.** Retrieval precision as a function of SNR and spectral resolution for simulated clear-  
 3 sky and all-sky retrievals. SNR and spectral resolution are set to vary from 50 to 250 and from  
 4 0.10 to 0.30 cm<sup>-1</sup>, respectively. The a priori is biased 3% from the truth and has a 3% uncertainty  
 5 for all species.